# A Bayesian Spatial Model to Correct Under-Reporting in Urban Crowdsourcing

**Gabriel Agostini, Emma Pierson†, Nikhil Garg†**

Cornell Tech, New York, United States

gsagostini@infosci.cornell.edu, emma.pierson@cornell.edu, ngarg@cornell.edu

**Abstract**

Decision-makers often observe the occurrence of events through a reporting process. City governments, for example, rely on resident reports to find and then resolve urban infrastructural problems such as fallen street trees, flooded basements, or rat infestations. Without additional assumptions, there is no way to distinguish events that occur but are not reported from events that truly did not occur–a fundamental problem in settings with positive-unlabeled data. Because disparities in reporting rates correlate with resident demographics, addressing incidents only on the basis of reports leads to systematic neglect in neighborhoods that are less likely to report events. We show how to overcome this challenge by leveraging the fact that events are *spatially correlated*. Our framework uses a Bayesian spatial latent variable model to infer event occurrence probabilities and applies it to storm-induced flooding reports in New York City, further pooling results across multiple storms. We show that a model accounting for under-reporting and spatial correlation predicts future reports more accurately than other models, and further induces a more equitable set of inspections: its allocations better reflect the population and provide equitable service to non-white, less traditionally educated, and lower-income residents. This finding reflects heterogeneous reporting behavior learned by the model: reporting rates are higher in Census tracts with higher populations, proportions of white residents, and proportions of owner-occupied households. Our work lays the groundwork for more equitable proactive government services, even with disparate reporting behavior.

## 1 Introduction

Urban crowdsourcing is key to identifying and resolving problems such as fallen street trees and flooded basements, in both emergency and daily contexts. For example, New York City's 311 system received over 3 million service requests in 2021 (NYC Open Data 2023). However, reporting is *heterogeneous* – different neighborhoods, even when facing similar problems, report problems at different rates (Liu, Bhandaram, and Garg 2023; Kontokosta, Hong, and Korsberg 2017; Minkoff 2016; O'Brien et al. 2017), and under-reporting often correlates with socioeconomic factors such as race, ethnicity, and income. If agencies primarily address incidents that are reported, then under-reporting leads to downstream disparities. This mistargeting of resources, especially when it results in inequity, is a substantial concern and is a stated priority research area for the Federal Emergency Management Agency (FEMA) in the United States (Federal Emergency Management Agency 2023).

While previous work has quantified the magnitude of reporting disparities, they do not estimate the probability that an event truly occurred at each location, which is essential for resource allocation. A challenge in estimation is that, without further assumptions, *unreported* incidents cannot be distinguished from incidents which *did not occur*. This is analogous to *positive-unlabeled* (PU) machine learning (Liu et al. 2003; Shanmugam and Pierson 2021), where datapoints are either labeled positive or unlabeled, and the latter group consists of both true positives and negatives.

PU learning problems are unsolvable without further assumptions on the data generating process (Bekker and Davis 2020). How do we make progress? Our insight is that many urban phenomena are *spatially correlated*, and we can use this correlation to distinguish under-reporting from true lack of event occurrence. For example, in our empirical application, we use reporting data for *flooding* after a storm. If an area does not report flooding but all of its spatial neighbors do, that area is likely to have experienced flooding (but not reported it); conversely, if no neighbors report flooding, that area is not likely to have experienced flooding. Spatial correlation departs from the standard PU learning setup, where the data points are assumed to be independent.

To encode spatial correlations, we build on top of a spatial Bayesian model developed in the ecology literature (Spezia, Friel, and Gimona 2018). The model uses a latent indicator variable at each location to encode whether an event truly occurs there; latent variables at adjacent locations are spatially correlated according to an Ising model (Onsager 1944). If an event does occur, the probability it generates an (observed) report varies as a function of location demographics. In semi-synthetic simulations, we show that the model infers where events have truly occurred more accurately than baseline models. For example, the model significantly outperforms a Gaussian Process (GP) in terms of AUC with an improvement of $0.14$.

Using this model, we develop a novel framework to iden-

*†Co-senior author

tify non-reported events in urban crowdsourcing and show it leads to more efficient and equitable resource allocation. We apply the framework to street flooding reports after storms in New York City obtained from public 311 data (NYC Open Data 2023). NYC uses such report data to allocate post-storm resources, such as addressing wood debris, clogged catch basins, or building water leaks (City of New York 2023). Storms cause severe damage; Hurricane Ida in 2021 was responsible for the largest rainfall hour in the city's history, over 7 billions of dollars in damage to infrastructure and the transportation system, and at least 13 deaths, heavily skewed along socioeconomic lines (Newman 2021).

Our framework—which accounts for both heterogeneous under-reporting and spatial correlation—outperforms baseline approaches in terms of *efficiency*: using report data immediately after the storm, it better predicts reports made days later. Such prediction can facilitate a more timely allocation of resources. Our framework also leads to more *equitable* allocation of inspections: the allocations are more in line with population proportions, as opposed to other models that are likely to rate minority and lower-income neighborhoods as lower priority for inspections, due to under-reporting. Finally, we show how to pool model estimates *across* storms to learn historical heterogeneous reporting patterns: we find that reporting rates are higher in Census tracts with higher median incomes, proportions of white residents, and proportions of owner-occupied housing.

Overall, our work (a) leverages spatial correlation in a Bayesian machine learning model to overcome the positive-unlabeled challenge in crowdsourcing; (b) develops a framework to validate and apply the model for more efficient and equitable emergency management response to a given storm event, and to pool reports across storms to identify under-reporting patterns; (c) applies the framework to real-world data, showing that it can substantially improve both the efficiency and equity of government responses to crowdsourcing. Our framework can improve responses in other contexts with spatial correlation, such as in public health and power outages. Together, we provide and validate a novel approach to resource *allocation* in the presence of under-reporting.

We further provide an open-source Python implementation of our approach for application in other contexts[1].

## 2 Related Work

Our work relates to multiple threads of prior literature from PU Learning, Bayesian methods in ecology, flood prediction, and urban crowdsourcing.

Our setting is one with **positive-unlabeled** data. Without further assumptions, even the proportion of true positive points—the *prevalence*—is unidentifiable because a positive-class, unlabeled data point is indistinguishable from a negative-class point. Hence, PU learning methods *must* make further assumptions (Bekker and Davis 2020); e.g., a common assumption is that each true positive point has the same uniform probability of being labeled positive (Elkan and Noto 2008). Even this strong assumption, which often does not hold in real-world settings where the labeling probability is non-uniform (e.g. when reporting is heterogeneous), is not sufficient. In contrast, our work overcomes the challenge by leveraging *spatial correlation*.

Methodologically, our work builds on approaches from the **ecology** literature, which seeks to count animal populations in the presence of detection errors (Heikkinen and Hogmander 1994; Sicacha-Parada et al. 2021; Della Rocca and Milanesi 2022; Xu et al. 2023). Santos-Fernandez et al. (2021) fit a Bayesian model to correct for misreporting errors in coral detection, leveraging spatial correlation and individuals that analyze coral in multiple locations. Most relevant is work by Spezia, Friel, and Gimona (2018). Their model assumes that the true probability of animal species presence is described by an Ising model, and observed presence is described by a reporting process. We build a framework to effectively use and validate this approach in urban crowdsourcing, showing that the model is predictive of future reports, can guide equitable resource allocation, and can be pooled across multiple events.

This work's specific empirical application – urban flood detection – is complementary to the substantial machine learning work on **flood prediction**, using precipitation and seasonal climate information and data from satellites or sensors (see Mosavi, Ozturk, and Chau (2018) for a comprehensive review). Mauerman et al. (2022), for example, use a Bayesian latent variable model to predict seasonal floods in Bangladesh through the reconstruction of historical satellite data. Agonafir et al. (2022) study infrastructure correlates of flooding using 311 reports in NYC. We believe that reporting data is a valuable complementary data source to sensors and satellites, and is especially temporally and spatially granular in urban environments; however, for both efficiency and equity, it is important to quantify and correct heterogeneous under-reporting. Future work could incorporate such outside sensor data into our model. Our approach is also applicable to reporting contexts beyond flooding.

There is a large literature quantifying disparities in **urban crowdsourcing**; a consistent challenge is disambiguating between low reporting rates and low ground truth rates. Liu, Bhandaram, and Garg (2023) show that time-stamped, duplicate reports about the same event can be used to identify the reporting process; O'Brien, Sampson, and Winship (2015) send researchers to neighborhoods to document ground-truth conditions. We contribute a method that leverages spatial correlation and, unlike other methods, *predicts* the probability an event has occurred in each location.

Finally, our work relates to a much broader literature on methods to quantify and compensate for the effects of missing and imperfect data in inequality-related contexts, including healthcare, policing, education, and government inspections (Coston, Rambachan, and Chouldechova 2021; Rambachan et al. 2021; Movva et al. 2023; Franchi et al. 2023; Laufer, Pierson, and Garg 2022; Guerdan et al. 2023; Zink, Obermeyer, and Pierson 2023; Cai et al. 2020; Pierson 2020; Liu, Rankin, and Garg 2024; Balachandar, Garg, and Pierson 2023; Obermeyer et al. 2019; Kleinberg et al. 2018; Zanger-Tishler, Nyarko, and Goel 2023; Jung et al. 2018; Garg, Li, and Monachou 2021; Lakkaraju et al. 2017; Arnold, Dobbie, and Hull 2022). This broader literature considers many

[1] Available at github.com/gsagostini/networks_underreporting/

types of missingness besides the PU-missingness we study here, and many types of identification approaches besides the spatial correlations leveraged here.

# 3 Model, Inference, and Framework

Our model captures three characteristics common to many urban crowdsourcing systems: (a) the city does not observe *ground truth* data (where incidents actually occurred), only *reports*; (b) there is *under-reporting*, i.e., not all incidents are reported, and under-reporting may be *heterogeneous* across demographic groups; (c) incidents are *spatially correlated*.

Formally, consider a network $G$ with $N$ nodes and adjacency matrix $E$. Each node $i$ has two binary state variables. First, $A_i \in \{-1, +1\}$ denotes the latent, ground-truth state; second, $T_i \in \{0, 1\}$ denotes the observed, reported state. In the flood setting, $A_i = 1$ if a flood occurred in that node and $-1$ if not, while $T_i = 1$ denotes that there was a report for flooding at the node. We observe reports $T_i$ and the network $G$, but not incidents $A_i$.

Our specific approach follows that of Spezia, Friel, and Gimona (2018). **Ground truth states** $A_1, \dots A_N$ are generated according to an Ising model with two real-valued parameters, $\theta_0$ and $\theta_1$, controlling the event *incidence rate* and spatial *correlation* respectively. The probability distribution of the vector $\vec{A} \in \{\pm 1\}^N$ is:

$$\Pr(\vec{A}) = \frac{\exp\left(\theta_0 \sum_i A_i + \theta_1 \sum_{i,j} A_i A_j \cdot E_{ij}\right)}{\mathcal{Z}(\theta_0, \theta_1)} \tag{1}$$

where $\mathcal{Z}(\theta_0, \theta_1)$ is an intractable *partition function* ensuring the distribution is normalized. As proven by Besag (1974), the conditional distribution for a single node $A_i$ given all other nodes, is, with positive spatially correlation $\theta_1 > 0$:

$$\begin{aligned}\Pr(A_i = 1 \mid A_k \; \forall\, k \neq i) \\ = \frac{1}{1 + \exp\left(-2\left(\theta_0 + \theta_1 \sum_j A_j \cdot E_{ij}\right)\right)}\end{aligned} \tag{2}$$

A **report** at node $i$ only depends on the incident state at $i$ and a *reporting rate* $\psi_i$, i.e.,

$$\Pr(T_i = 1 \mid A_i = 1) = \psi_i. \tag{3}$$

As in PU learning, we assume that there are no false positive reports: $\Pr\left(T_i = 1 \mid A_i = -1\right) = 0$.

We fit and compare two models for reporting rates $\psi_i$:

- With **homogeneous reporting**, $\psi_i = \alpha$ is assumed constant across nodes.
- With **heterogeneous reporting**, report rates $\psi_i$ are a function of demographic factors of node $i$. That is, given $M$ node-specific features $X_{i1} \dots X_{iM}$,

$$\psi_i = \text{logit}^{-1}\left(\alpha_0 + \sum_{\ell=1}^{M} \alpha_\ell X_{i\ell}\right), \tag{4}$$

  where the coefficients $\alpha_0, \dots \alpha_M$ are learned latent parameters shared across nodes.

We discuss some of the modeling choices in Section 7.

## 3.1 Inference procedure

Given reporting data $\{T_i\}$ and a spatial network with known edges $\{E_{ij}\}$, we use a Gibbs sampling MCMC procedure for posterior inference: namely, at each iteration, we draw each latent value from its conditional distribution given the current values of all the other variables. All variables are initialized at random. Model priors are in Appendix F.

We provide code with our submission – we note that we modify the procedure of Spezia, Friel, and Gimona (2018), to speed up inference, such as by jointly sampling some of the parameters within the outer Gibbs routine and implementing dynamic step size optimization. We believe that the public Python code release will enable other practitioners in crowdsourcing or ecology settings to apply such methods.

**Sampling $\theta_0$ and $\theta_1$:** The conditional distribution of $\theta_0$ and $\theta_1$ given all other variables depends only on $\vec{A}$. We cannot directly compute it due to the presence of the partition function $\mathcal{Z}$ in eq. (1) (Murray, Ghahramani, and MacKay 2006). This normalization constant is intractable, as it must be evaluated for $2^N$ values of the ground-truth vector $\vec{A}$.

We use the Single-Variable Exchange Algorithm (SVEA) to circumvent this difficulty (Møller et al. 2006). The SVEA is a Metropolis-Hasting type sampling algorithm that introduces an auxiliary variable $\vec{w}$ to cancel two terms with the partition function when computing the acceptance ratio. To do so, $\vec{w}$ must be sampled from the same distribution family as $\vec{A}$. We generate auxiliary variables from the Ising model distribution in eq. (1) using the Swendsen-Wang algorithm with 50 burn-in samples (Swendsen and Wang 1987; Wolff 1989). This is an efficient method to sample from an Ising Model with $\theta_1 > 0$ (Park et al. 2017; Cooper et al. 2000).

**Sampling $A_i$:** We sample each of the $A_i$ through Gibbs sampling. The conditional distribution of $A_i$ depends on $\theta_0$, $\theta_1$, $T_i$, and $A_j$ for $j$ such that $E_{ij} = 1$. If the corresponding $T_i = 1$, then the no false positives assumption leads to $\Pr(A_i = 1 \mid \cdot) = 1$. Otherwise, $\Pr(A_i \mid \cdot)$ is the conditional probability implied by eqs. (2) and (3).

**Sampling $\psi_i$:** In the *homogeneous reporting model*, we fit a single parameter $\alpha$ to describe the reporting rate. Given a beta prior, the conditional distribution of $\alpha$ is a beta distribution depending on the numbers of incidents that 1) occurred and are reported and 2) occurred and are not reported.

In the *heterogeneous reporting model*, the conditional distribution for the coefficients $\alpha_0, \dots \alpha_M$ can be found by fitting a Bayesian logistic regression of the reports $T_i$ on the demographic features, restricted to the nodes for which the current latent ground truth parameters are positive ($A_i = 1$). We compute $\psi_i$ following eq. (4).

**Sampling hyper-parameters.** We draw 3 chains with 40,000 samples each, after 20,000 burn-in samples. During burn-in, we optimize the auxiliary variable sampling step size. Further hyper-parameters are described on Appendix F.

**Inferred values.** Our procedure gives posterior samples for each of $\theta_0, \theta_1, \alpha_\ell$ (and thus induced $\psi_i$), and $A_i$. We use these parameters to calculate $\Pr(A_i = 1 | \cdot)$.

### 3.2 Framework overview

We use the above model as a foundation and present a novel framework for resource allocation in the presence of under-reporting. Our framework for evaluation and application, implemented in the remainder of the paper, is as follows.

First, we evaluate the approach *semi*-synthetically using the real spatial map, showing model expressivity (that it can generate the full range of storm data), parameter recovery (that estimated parameter point estimates are correct and posteriors are calibrated), and predictive performance (that it correctly identifies unreported events $A_i$).

Second, we evaluate performance on real storm data, without needing external ground truth data. In particular, we show that, using data in the initial hours after the storm, the model predicts *future* reports in the following days.

Third, we demonstrate the approach's *application* to more efficient and equitable resource allocation. We show that, using the model predictions of ground truth unreported events $P(A_i)$, the resulting allocation better matches the population distribution and in particular does not deprioritize populations with lower reporting rates, unlike other approaches.

Finally, we *pool* parameters across storms (using a Bayes factor approach as described in Appendix A.1) to robustly characterize under-reporting behavior over time. Leveraging estimates of under-reporting behavior across storms would further aid in proactive resource allocation for future storms.

## 4 Data and models

**Data.** We apply our model to flood reports in New York City. We primarily use Census tracts as nodes in our graph; two tracts are adjacent if they share a border. Minimum-distance edges are drawn whenever needed to make the graph connected (e.g. linking Staten Island to Brooklyn). For node-specific features $X$, we use demographic variables obtained from Census data, which include population, socioeconomic status, and racial composition measurements.

We use 311 resident reports of street floods. For our main results, we look at reports in the week of September 1st through September 8th, following Hurricane Ida. The 311 reports dataset is publicly available in the NYC Open Data portal, supporting replication of our results. We split the data into train and test reporting periods: we fit our models with reports created until $8\%$ of the census tracts have received at least one report—this threshold is reached around 4 hours after the storm starting time. The remaining reports are used for evaluation. Out of the 2221 census tracts in our network, 177 tracts report at least one flooding incident during the training period, and 346 tracts report during the test period.

When evaluating historical under-reporting, we also consider reports of other floods in New York City. We look at data following the passage of Hurricane Henri (August 2021) and Tropical Storm Ophelia (September 2023). Further details on reports and data are presented in Appendix G.

**Models evaluated.** We present results from four models: (a) Our model with *homogeneous reporting*; (b) Our model with *heterogeneous reporting*, with reporting probability varying as a function of demographic features; (c) a *spatial baseline* model in which we predict test-time reporting as the fraction of a node's neighbors that reported during training period; (d) a *Gaussian Process* (GP) baseline model, a standard approach to leverage geographic information. The baselines reflect approaches to incorporating spatial correlation, without explicitly modeling the reporting process as distinct from the incident occurrence process. Other modeling approaches (such as graph neural networks) may also be appropriate and perform well in terms of prediction, but it may be challenging to use such models to separately recover reporting from ground truth processes – we leave such approaches to future work.

## 5 Semi-synthetic simulation experiments

We verify that our models correctly recover the true parameters and latent states in semi-synthetic data settings where the ground truth parameters and latent state are known. To generate semi-synthetic data, we begin with the real NYC spatial network $E$ and demographic features $X$, and then for each of the two reporting models (homogeneous and heterogeneous), we generate latent states $A$ and reports $T$ through MCMC sampling assuming the corresponding data generating process. The observed data given to each model is $T$, $E$, and (for the heterogeneous reporting model) $X$. For all experiments, 500 trials were performed; for each trial, we resample new values of the latent parameters, re-generate $A$ and $T$, and run two MCMC chains for inference. Here, we report results when data is drawn according to the heterogeneous model; details and other results, including validating model expressivity, are in Appendix D.

**Calibration and Identifiability.** We verify that our inference procedure correctly recovers the true data generating parameters, a standard identifiability check (Chang et al. 2021; Pierson et al. 2019). We find an overall high correlation between the recovered parameters and the true, latent parameter values. Correlation values all $0.60$. For the regression slope coefficients $\alpha_\ell$, which we more directly analyze, correlations of $0.91$ and higher are observed. We also verify that our confidence intervals are *calibrated*, another standard check (Wilder, Mina, and Tambe 2021): at each significance level, whether posterior distribution confidence intervals cover the correct fraction of true values.

**Predictive Performance.** An advantage of semi-synthetic data (in contrast to real data) is that the ground truth latent states $A_i$ are known. We can therefore compare the model's inferred event probabilities $\Pr(A_i)$ to the true latent states $A_i$. Table 1 reports model AUC (area under the ROC curve), comparing the heterogeneous reporting model to the baselines and the homogeneous model *when data is drawn following the heterogeneous model*. We find that correctly accounting for heterogeneous under-reporting has strong predictive performance, increasing increases AUC by $0.122$ from the homogeneous reporting model, by $0.129$ from the spatial baseline, and by $0.142$ from the GP baseline—all at a significance level of $10^{-4}$ or less. These values are repeated alongside analogous results for RMSE in Appendix Table 4.

Overall, our semi-synthetic experiments validate that our model correctly recovers the true latent parameters, includ-

| Model | AUC | 95% CI |
|---|---|---|
| Heterogeneous Reporting | 0.642 | (0.637, 0.647) |
| Homogeneous Reporting | 0.520 | (0.515, 0.525) |
| GP Baseline | 0.501 | (0.497, 0.505) |
| Spatial Baseline | 0.513 | (0.509, 0.518) |

Table 1: In simulation, average AUC to predict latent ground-truth $A_i$ according to each model. Nodes with observed training reports are excluded, as they are perfectly predicted by all models by definition. Confidence intervals were obtained through bootstrapping with 10,000 iterates.

ing how demographic covariates influence reporting rates. In this way, the use of spatial correlation overcomes the PU learning identifiability challenge. Further, our model outperforms baselines in the ability to infer the unobserved ground truth states $A_i$. Finally, the simulations demonstrate that, when true reporting processes are heterogeneous, assuming homogeneous under-reporting worsens estimation.

## 6 Empirical Results

We now apply our framework to NYC 311 data. First, we fit the models to training report data from Hurricane Ida and show that our models outperform the baseline in terms of *efficiency*, i.e., predicting future reports. Then, we show that accounting for heterogeneous under-reporting leads to *more equitable* allocation of resources. Finally, looking at results across multiple storms, we investigate the socioeconomic and demographic features that are mostly associated with heterogeneity in under-reporting.

**Prediction of floods and future reports.** Figure 1 shows, for the *heterogeneous reporting model*, the inferred probability of flood by census tract, $\Pr(A_i)$. This map indicates that there is a substantial spatial correlation in reporting, but also that there is likely substantial under-reporting: many tracts have several neighboring tracts with reports, but did not report themselves. The positive spatial correlation is captured by our positive estimate for the spatial correlation parameter $\theta_1$ (0.15, 95% CI (0.08, 0.21)). Convergence diagnostics indicate that the inference procedure converged, with maximum $\hat{R} = 1.03$ for the latent parameters.

We evaluate the four models by how well they predict *future reports.* Unlike the simulation results discussed in Section 5, we cannot evaluate the models in terms of predicting ground truth $A_i$: we do not have access to *true* flooding events, just reports – lack of such ground truth data indeed motivates the city to use 311 reporting data. We fit the model using train time data and then compare the model estimates of $\Pr(T)$ to future reports $T$ during the test period. This prediction task is decision-relevant because better prediction of future reports would allow the agency to proactively allocate resources (though, as we discuss below, the agency should still be aware of heterogeneous under-reporting).

Table 2 reports AUC and RMSE for each model, along with bootstrapped 95% confidence intervals and relative improvements. The models accounting for under-reporting achieve better predictive performance than the baseline

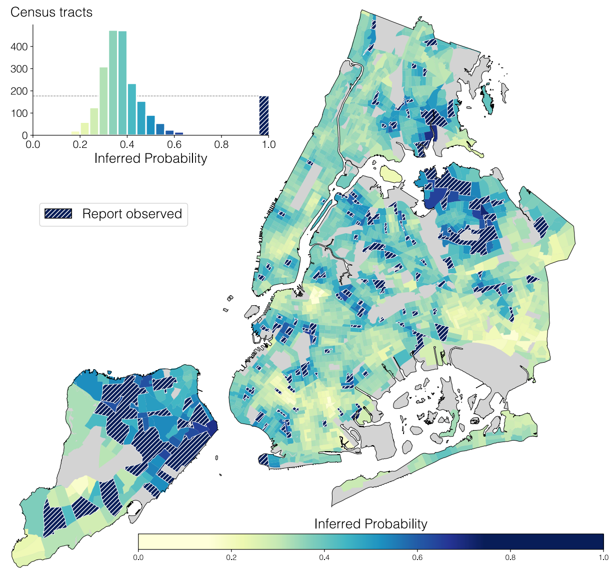


Figure 1: Model-inferred probabilities $\Pr(A_i)$ that each New York City Census tract is flooded after Hurricane Ida, from the heterogeneous reporting model. Hatched lines indicate tracts that reported during the training period.

models that do not. The p-values shown test for positive *differences* between each pair of models. Performance improvements are statistically significant at the 0.05 level for each of our models over the baselines. In practice, an improvement in report prediction – when converted to estimates of ground truth $A_i$ – would translate to more efficient resource allocation, as city governments can anticipate what areas will need attention after a disaster.

**Equitable inspection allocation.** Consider an agency that is allocating resources (such as emergency response, maintenance, or inspections) after storms, in response to reports. Table 2 suggests that our models could lead to more *efficient* allocations, as they are more predictive of future reports after the first day. Here, we analyze how *equitable* these allocations are, under each of the three models we study. We consider the task of allocating a fixed number of resources to Census tracts without reports ($T_i = 0$) – as most tracts receive no report, the agency can allocate some resources to such tracts. We suppose that the agency first infers flood probabilities $\Pr(A_i)$ for each tract in which no report was received, $T_i = 0$. It then allocates resources to the $k$ tracts with the highest inferred probabilities $\Pr(A_i)$.

Figure 2 shows the fraction of resources allocated to non-white residents and residents without a high school degree, when $k = 100$, alongside the population fractions of the tracts without a report. The model accounting for heterogeneous reporting allocates resources more in line with the population distribution, especially in comparison to the homogeneous reporting model which accounts for under-reporting but not *differences* between populations. Note that

| Model | AUC Estimate | AUC 95% CI | RMSE Estimate | RMSE 95% CI |
|---|---|---|---|---|
| Heterogeneous Reporting | 0.680 | (0.646, 0.713) | 0.355 | (0.338, 0.371) |
| Homogeneous Reporting | 0.682 | (0.649, 0.714) | 0.360 | (0.343, 0.376) |
| GP Baseline | 0.629 | (0.595, 0.662) | 0.417 | (0.400, 0.434) |
| Spatial Baseline | 0.647 | (0.616, 0.678) | 0.395 | (0.377, 0.412) |

(a) AUC and RMSE point estimates and confidence intervals for each of the four models.

| Model A | Model B | $\Delta_{\text{AUC}}$ | $\Delta_{\text{AUC}}$ p-value | $\Delta_{\text{RMSE}}$ | $\Delta_{\text{RMSE}}$ p-value |
|---|---|---|---|---|---|
| Heterogeneous Reporting | Homogeneous Reporting | -0.002 | 0.831 | -0.004 | 0.004 |
| | GP Baseline | 0.051 | 0.003 | -0.062 | $< 10^{-3}$ |
| | Spatial Baseline | 0.033 | 0.009 | -0.040 | $< 10^{-3}$ |
| Homogeneous Reporting | GP Baseline | 0.054 | $< 10^{-3}$ | -0.058 | $< 10^{-3}$ |
| | Spatial Baseline | 0.035 | $< 10^{-3}$ | -0.035 | $< 10^{-3}$ |

(b) AUC and RMSE changes. Two-sided p-values report whether model A and model B differ significantly in performance.

Table 2: Performance metrics for the four models in predicting future reports. Confidence intervals were obtained by bootstrapping the tracts with 10,000 iterates.

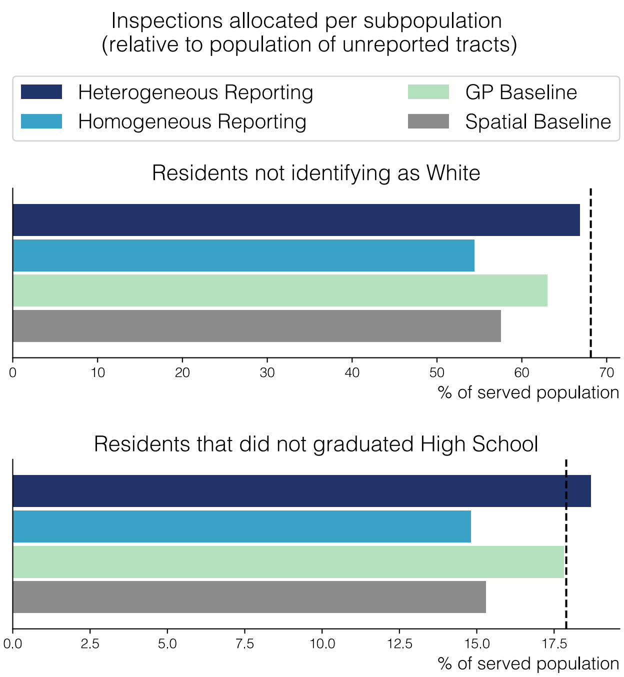


Figure 2: Demographic disparities when allocating resources to 100 census tracts (among those that do not report), using inferred flood probabilities from the four models. The horizontal axes shows the proportion of all residents served by the inspections (i.e. those who reside in the 100 inspected census tracts) who are non-white and do not have a high school degree, computed as a weighted average from the proportions on inspected tracts. Dashed lines represent the total proportion of residents in tracts without a report who are non-white and do not have a high school degree.

the model does so while achieving similar predictive performance, as established above.

Additional results in Appendix E show these results are robust to other values of $k$ and for other socioeconomic and demographic factors. The results establish that taking into account heterogeneous under-reporting leads to less deprioritization of non-white and socioeconomically disadvantaged populations (more in line with population distributions).

**Socioeconomic factors of heterogeneous reporting.** Figure 2 suggests that the heterogenous reporting model identifies and corrects for demographic disparities in under-reporting. We now analyze such differences directly. To understand *persistent* reporting behavior across storms, we also run our model for Hurricanes Ophelia (September 2023) and Henri (August 2021) and pool together the feature coefficients. The pooling method and (qualitatively identical) results for individual storms are in Appendix A.

Using the pooled regression coefficients, we estimate report rates $\psi_i$ for each census tract, with results shown in Figure 3. Demographic patterns emerge – e.g., the Upper West and Upper East Side neighborhoods in Manhattan, with higher median incomes, are estimated to have a higher reporting rate $\psi_i$ than surrounding areas, even though few reports were received in those areas. In contrast, the Bronx (relatively lower incomes) is estimated to have a low reporting rate. Taking a weighted average across neighborhoods, the reporting rate for white populations is, on average: 24% higher than Black populations, 18% higher than Hispanic populations, and 12% higher than Asian populations.

Next, we ask: what demographic factors are associated with under-reporting? Figure 4 shows the pooled posteriors for each coefficient $\alpha_\ell$ in equation 4: population, income, education, race/ethnicity, age, and household ownership.

We find that there are significant demographic disparities in reporting. As expected, a higher population is associated with higher reporting rates. However, other demographic factors are also associated with reporting rates. Higher proportions of white residents are positively correlated with reporting rate even when controlling for the other five demographic features considered, consistent with the different average report rates per subpopulation shown in Figure 3. Median age and fraction of households occupied by a renter are negatively correlated with higher reporting, suggesting that neighborhoods with older, home-owning populations tend to receive reports at a higher rate. These estimates are consistent with prior work on demographic disparities in reporting in the NYC 311 system (Liu, Bhandaram, and Garg 2023). These estimates further explain the results in Figure 2: the heterogeneous reporting model can identify and correct for these reporting disparities when calculating $P(A_i|\cdot)$, the probability that an area is actually flooded (even when no one submitted a report).

Further discussion, as well as similar analyses for other features, is in Appendix C.

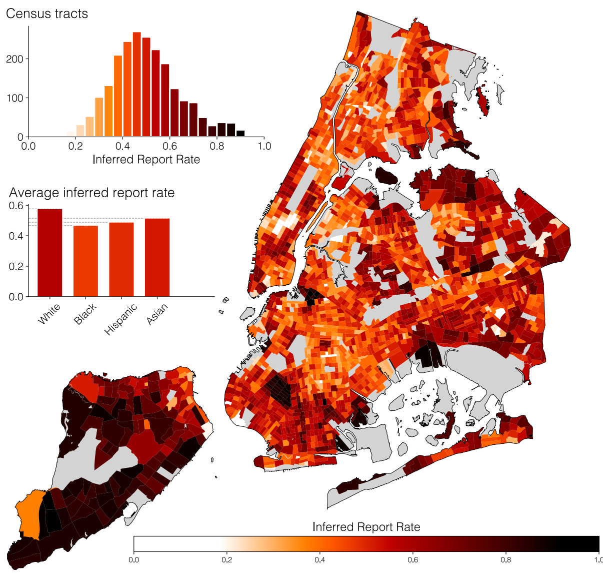


Figure 3: Model-inferred report rates $\psi_i$ per census tract, from the heterogeneous reporting model. The report rates range from near $0.1$ to $0.9$. Weighted averages of report rates per racial composition are shown in a bar plot.

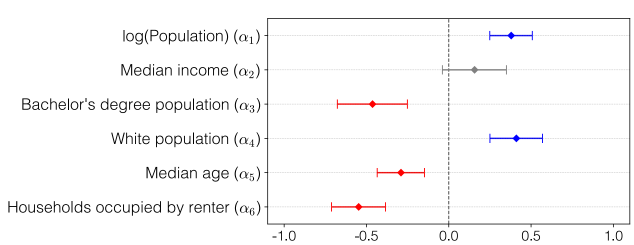


Figure 4: Estimated multivariate coefficients after pooling the three storms. Features were all standardized. Confidence intervals shown, and estimates with insignificant non-zero association colored in grey.

## 7 Discussion

This work shows the promise of leveraging the *spatial correlation* of incidents to quantify and correct for *under-reporting* in city crowdsourcing systems. Using a case study of flood reporting in New York City, we show that a Bayesian spatial model can accurately recover ground truth under-reporting patterns on semi-synthetic data by leveraging spatial correlation—a challenging task in missing data (PU learning) settings like the one we study. Using this model, we develop a framework for more accurate prediction of future flood reports compared to baselines, and allocation of resources that are more in line with population proportions (not neglecting neighborhoods with larger proportions of non-white and lower-income residents) – improving both efficiency and equity.

Future work might extend the model in several directions. (1) First, we fit the model on binarized reporting data: i.e., whether a location has *any reports*, as opposed to the *count* of reports. While, in our setting, a binary variable is sufficient to capture most of the variation (96.5% of locations have zero or one report) the modeling approach here could plausibly be extended to accommodate count data as well. (2) Second, we assume that flooding is spatially correlated according to an Ising model, and do not explicitly model shared infrastructure and weather patterns. We adopt this model given the well-studied nature of Ising models, which aids estimation. Future work – as driven by the model setting – may choose to modify these choices, though model identifiability may be a challenge. (3) Third, in crowdsourcing settings, we can sometimes incorporate external data, such as (potentially noisy or non-randomly distributed) sensors. That is: if we have access to data from a different source (e.g. sensors to detect floods that are placed sparsely through the city) which reveals that $A_i = 1$ even though $T_i = 0$ for some $i$, will estimates improve? This question is practically important: often inspections occur in clusters of regions, and it would be important for decision-makers to be able to incorporate the results of negative inspections in the model. (4) Fourth, 311 data is richer than data in other under-reporting settings (such as in ecology) due to spatiotemporal correlations in reporting rates across different incident types or different events of the same type. For example, report rates for flood events may be related to report rates for pest infestations or noise complaints, as both may be related to socioeconomic or other factors. We further note that we can use the pooled estimates of reporting rates across storms when new storms occur, leading to faster, more efficient and equitable allocation. All of these directions represent important opportunities for future work.

## 8 Acknowledgments


The authors thank Sidhika Balachandar, Serina Chang, Zhi Liu, Allison Koenecke, Matt Franchi, and Arkadiy Saakyan for feedback. This research was supported by a Meta research award, Google Research Scholar award, a Cornell Tech Urban Tech grant, NSF CAREER #2142419, a CIFAR Azrieli Global scholarship, a LinkedIn Research Award, and the Abby Joseph Cohen Faculty Fund.


## References


Agonafir, C.; Pabon, A. R.; Lakhankar, T.; Khanbilvardi, R.; and Devineni, N. 2022. Understanding New York City street flooding through 311 complaints. *Journal of Hydrology*, 605: 127300.

Arnold, D.; Dobbie, W.; and Hull, P. 2022. Measuring racial discrimination in bail decisions. *American Economic Review*, 112(9): 2992–3038.

Balachandar, S.; Garg, N.; and Pierson, E. 2023. Domain constraints improve risk prediction when outcome data is missing. *NeurIPS ML4H Symposium*.

Bekker, J.; and Davis, J. 2020. Learning from positive and unlabeled data: a survey. *Machine Learning*, 109(4): 719–760.

Besag, J. 1974. Spatial Interaction and the Statistical Analysis of Lattice Systems. *Journal of the Royal Statistical Society: Series B (Methodological)*, 36(2): 192–225.

Cai, W.; Gaebler, J.; Garg, N.; and Goel, S. 2020. Fair allocation through selective information acquisition. In *Proceedings of the AAAI/ACM Conference on AI, Ethics, and Society*, 22–28.

Chang, S.; Pierson, E.; Koh, P. W.; Gerardin, J.; Redbird, B.; Grusky, D.; and Leskovec, J. 2021. Mobility network models of COVID-19 explain inequities and inform reopening. *Nature*, 589(7840): 82–87.

City of New York. 2023. Severe Weather.

Cooper, C.; Dyer, M. E.; Frieze, A. M.; and Rue, R. 2000. Mixing properties of the Swendsen–Wang process on the complete graph and narrow grids. *Journal of Mathematical Physics*, 41(3): 1499–1527.

Coston, A.; Rambachan, A.; and Chouldechova, A. 2021. Characterizing fairness over the set of good models under selective labels. In *International Conference on Machine Learning*, 2144–2155. PMLR.

Della Rocca, F.; and Milanesi, P. 2022. The New Dominator of the World: Modeling the Global Distribution of the Japanese Beetle under Land Use and Climate Change Scenarios. *Land*, 11(4): 567. Number: 4 Publisher: Multidisciplinary Digital Publishing Institute.

Elkan, C.; and Noto, K. 2008. Learning classifiers from only positive and unlabeled data. In *Proceedings of the 14th ACM SIGKDD international conference on Knowledge discovery and data mining*, KDD '08, 213–220. New York, NY, USA: Association for Computing Machinery. ISBN 978-1-60558-193-4.

Federal Emergency Management Agency. 2023. Appendix 2 - Learning Agenda. https://www.fema.gov/about/strategic-plan/appendices/learning-agenda.

Franchi, M.; Zamfirescu-Pereira, J.; Ju, W.; and Pierson, E. 2023. Detecting disparities in police deployments using dashcam data. In *Proceedings of the 2023 ACM Conference on Fairness, Accountability, and Transparency*, 534–544.

Garg, N.; Li, H.; and Monachou, F. 2021. Standardized tests and affirmative action: The role of bias and variance. In *Proceedings of the 2021 ACM Conference on Fairness, Accountability, and Transparency*, 261–261.

Guerdan, L.; Coston, A.; Holstein, K.; and Wu, Z. S. 2023. Counterfactual Prediction Under Outcome Measurement Error. In *Proceedings of the 2023 ACM Conference on Fairness, Accountability, and Transparency*, 1584–1598.

Heikkinen, J.; and Hogmander, H. 1994. Fully Bayesian Approach to Image Restoration with an Application in Biogeography. *Journal of the Royal Statistical Society. Series C (Applied Statistics)*, 43(4): 569–582. Publisher: [Wiley, Royal Statistical Society].

Jung, J.; Corbett-Davies, S.; Shroff, R.; and Goel, S. 2018. Omitted and included variable bias in tests for disparate impact. *arXiv preprint arXiv:1809.05651*.

Kleinberg, J.; Lakkaraju, H.; Leskovec, J.; Ludwig, J.; and Mullainathan, S. 2018. Human decisions and machine predictions. *The quarterly journal of economics*, 133(1): 237–293.

Kontokosta, C.; Hong, B.; and Korsberg, K. 2017. Equity in 311 Reporting: Understanding Socio-Spatial Differentials in the Propensity to Complain. ArXiv:1710.02452 [cs].

Lakkaraju, H.; Kleinberg, J.; Leskovec, J.; Ludwig, J.; and Mullainathan, S. 2017. The selective labels problem: Evaluating algorithmic predictions in the presence of unobservables. In *Proceedings of the 23rd ACM SIGKDD International Conference on Knowledge Discovery and Data Mining*, 275–284.

Laufer, B.; Pierson, E.; and Garg, N. 2022. End-to-end Auditing of Decision Pipelines. In *ICML Workshop on Responsible Decision-Making in Dynamic Environments. ACM, Baltimore, Maryland, USA*, 1–7.

Liu, B.; Dai, Y.; Li, X.; Lee, W.; and Yu, P. 2003. Building text classifiers using positive and unlabeled examples. In *Third IEEE International Conference on Data Mining*, 179–186.

Liu, Z.; Bhandaram, U.; and Garg, N. 2023. Quantifying spatial under-reporting disparities in resident crowdsourcing. *Nature Computational Science*.

Liu, Z.; Rankin, S.; and Garg, N. 2024. Identifying and Addressing Disparities in Public Libraries with Bayesian Latent Variable Modeling. In *Proceedings of the AAAI Conference on Artificial Intelligence*.

Mauerman, M.; Tellman, E.; Lall, U.; Tedesco, M.; Colosio, P.; Thomas, M.; Osgood, D.; and Bhuyan, A. 2022. High-Quality Historical Flood Data Reconstruction in Bangladesh Using Hidden Markov Models. In Tarekul Islam, G. M.; Shampa, S.; and Chowdhury, A. I. A., eds., *Water Management: A View from Multidisciplinary Perspectives*, 191–210. Cham: Springer International Publishing. ISBN 978-3-030-95722-3.

Minkoff, S. L. 2016. NYC 311: A Tract-Level Analysis of Citizen–Government Contacting in New York City. *Urban Affairs Review*, 52(2): 211–246. Publisher: SAGE Publications Inc.

Mosavi, A.; Ozturk, P.; and Chau, K.-w. 2018. Flood prediction using machine learning models: Literature review. *Water*, 10(11): 1536.

Movva, R.; Shanmugam, D.; Hou, K.; Pathak, P.; Guttag, J.; Garg, N.; and Pierson, E. 2023. Coarse race data conceals disparities in clinical risk score performance. *arXiv preprint arXiv:2304.09270*.

Murray, I.; Ghahramani, Z.; and MacKay, D. J. C. 2006. MCMC for Doubly-Intractable Distributions. In *Proceedings of the Twenty-Second Conference on Uncertainty in Artificial Intelligence*, UAI'06, 359–366. Arlington, Virginia, USA: AUAI Press. ISBN 0974903922.

Møller, J.; Pettitt, A. N.; Reeves, R.; and Berthelsen, K. K. 2006. An Efficient Markov Chain Monte Carlo Method for Distributions with Intractable Normalising Constants. *Biometrika*, 93(2): 451–458. Publisher: [Oxford University Press, Biometrika Trust].

Newman, A. 2021. 43 Die as Deadliest Storm Since Sandy Devastates the Northeast. *The New York Times*.

NYC Open Data. 2023. 311 Service Requests from 2010 to Present.

Obermeyer, Z.; Powers, B.; Vogeli, C.; and Mullainathan, S. 2019. Dissecting racial bias in an algorithm used to manage the health of populations. *Science*, 366(6464): 447–453.

Onsager, L. 1944. Crystal Statistics. I. A Two-Dimensional Model with an Order-Disorder Transition. *Physical Review*, 65(3-4): 117–149. Publisher: American Physical Society.

O'Brien, D. T.; Offenhuber, D.; Baldwin-Philippi, J.; Sands, M.; and Gordon, E. 2017. Uncharted Territoriality in Coproduction: The Motivations for 311 Reporting. *Journal of Public Administration Research and Theory*, 27(2): 320–335.

O'Brien, D. T.; Sampson, R. J.; and Winship, C. 2015. Ecometrics in the Age of Big Data: Measuring and Assessing "Broken Windows" Using Large-scale Administrative Records. *Sociological Methodology*, 45(1): 101–147.

Park, S.; Jang, Y.; Galanis, A.; Shin, J.; Stefankovic, D.; and Vigoda, E. 2017. Rapid Mixing Swendsen-Wang Sampler for Stochastic Partitioned Attractive Models. ArXiv:1704.02232 [cs, stat].

Pierson, E. 2020. Assessing racial inequality in COVID-19 testing with Bayesian threshold tests. *NeurIPS ML4H Workshop*.

Pierson, E.; Koh, P. W.; Hashimoto, T.; Koller, D.; Leskovec, J.; Eriksson, N.; and Liang, P. 2019. Inferring multidimensional rates of aging from cross-sectional data. In *The 22nd International Conference on Artificial Intelligence and Statistics*, 97–107. PMLR.

Rambachan, A.; et al. 2021. Identifying prediction mistakes in observational data. *Harvard University*.

Santos-Fernandez, E.; Peterson, E. E.; Vercelloni, J.; Rushworth, E.; and Mengersen, K. 2021. Correcting Misclassification Errors in Crowdsourced Ecological Data: A Bayesian Perspective. *Journal of the Royal Statistical Society Series C: Applied Statistics*, 70(1): 147–173.

Shanmugam, D.; and Pierson, E. 2021. Quantifying Inequality in Underreported Medical Conditions. *arXiv preprint arXiv:2110.04133*.

Sicacha-Parada, J.; Steinsland, I.; Cretois, B.; and Borgelt, J. 2021. Accounting for spatial varying sampling effort due to accessibility in Citizen Science data: A case study of moose in Norway. *Spatial Statistics*, 42: 100446.

Spezia, L.; Friel, N.; and Gimona, A. 2018. Spatial hidden Markov models and species distributions. *Journal of Applied Statistics*, 45(9): 1595–1615.

Suwardi, I. S.; Dharma, D.; Satya, D. P.; and Lestari, D. P. 2015. Geohash index based spatial data model for corporate. In *2015 International Conference on Electrical Engineering and Informatics (ICEEI)*, 478–483.

Swendsen, R. H.; and Wang, J.-S. 1987. Nonuniversal critical dynamics in Monte Carlo simulations. *Physical Review Letters*, 58(2): 86–88. Publisher: American Physical Society.

Wilder, B.; Mina, M.; and Tambe, M. 2021. Tracking Disease Outbreaks from Sparse Data with Bayesian Inference. *Proceedings of the AAAI Conference on Artificial Intelligence*, 35(6): 4883–4891.

Wolff, U. 1989. Collective Monte Carlo Updating for Spin Systems. *Physical Review Letters*, 62(4): 361–364. Publisher: American Physical Society.

Xu, L.; Rolf, E.; Beery, S.; Bennett, J. R.; Berger-Wolf, T.; Birch, T.; Bondi-Kelly, E.; Brashares, J.; Chapman, M.; Corso, A.; et al. 2023. Reflections from the Workshop on AI-Assisted Decision Making for Conservation. *arXiv preprint arXiv:2307.08774*.

Zanger-Tishler, M.; Nyarko, J.; and Goel, S. 2023. Risk scores, label bias, and everything but the kitchen sink. *arXiv preprint arXiv:2305.12638*.

Zink, A.; Obermeyer, Z.; and Pierson, E. 2023. Race Corrections in Clinical Models: Examining Family History and Cancer Risk. *medRxiv*, 2023–03.

# A Model Results for Other Storms

We repeat our empirical process for other storms, and then *pool* our estimates together across storms. In particular, we run our heterogeneous reporting model on two other New York City storms: Hurricane Henri (August 2021) and Tropical Storm Ophelia (September 2023). We compare our estimates across storms to each other, finding remarkable consistency. We further compare the results with those of (Liu, Bhandaram, and Garg 2023), who also estimate census tract-level reporting rates in NYC 311, though using a different method that leverages *duplicate* reports about the same incident.

## A.1 Method for Pooling results across storm events

A benefit of our Bayesian approach is that we can pool model estimates across storm events. While some parameters such as reporting intercepts ($\alpha_0$), overall flooding frequency ($\theta_0$), and spatial correlation ($\theta_1$) are likely to be storm specific, other reporting parameters $\alpha_\ell$ (representing effects of demographic or socioeconomic factors) may be relatively consistent across events. We thus pool our estimates across events to increase statistical power.

Pooling is done via a Bayesian model pooling approach. We assume that the data (reports for each node for a given storm) are conditionally independent across storms, given the model parameters and flood occurrence – i.e., whether a node (or two separate nodes) make reports in two separate events is not correlated, given the ground truth (similar to the assumption within each storm). Given this assumption, we can pool the results as follows.

For a given parameter $\alpha$ (for example, the coefficient corresponding to the population density or median income), suppose we have posterior distributions for a set of storms $\{1, \dots k, \dots K\}$ – i.e., given the report data $\vec{T}_k$ for each storm $k$, we have a posterior $\Pr(\alpha \mid \vec{T}_k)$. We want to estimate the posterior of the parameter given *all* the storm data, which is:

$$\Pr\left(\alpha \mid \vec{T}_1, \dots \vec{T}_K\right)$$

We do so as follows:

$$\begin{aligned}
\Pr\left(\alpha \mid \vec{T}_1, \dots \vec{T}_K\right) &= \frac{\Pr\left(\vec{T}_1, \dots \vec{T}_K \mid \alpha\right) \cdot \Pr(\alpha)}{\Pr\left(\vec{T}_1, \dots \vec{T}_K\right)} && \text{Bayes' rule} \\
&= \frac{\prod_{k=1}^{K} \left[\Pr\left(\vec{T}_k \mid \alpha\right)\right] \cdot \Pr(\alpha)}{\Pr\left(\vec{T}_1, \dots \vec{T}_K\right)} && \text{conditional indep.} \\
&= \prod_{k=1}^{K} \left[\frac{\Pr\left(\alpha \mid \vec{T}_k\right) \cdot \Pr\left(\vec{T}_k\right)}{\Pr(\alpha)}\right] \cdot \frac{\Pr(\alpha)}{\Pr\left(\vec{T}_1, \dots \vec{T}_K\right)} && \text{Bayes' rule} \\
&= C \cdot \prod_{k=1}^{K} \left[\frac{\Pr\left(\alpha \mid \vec{T}_k\right)}{\Pr(\alpha)}\right] \cdot \Pr(\alpha), \quad \text{where } C = \frac{\prod_{k=1}^{K} \Pr\left(\vec{T}_k\right)}{\Pr\left(\vec{T}_1, \dots \vec{T}_K\right)} && (5)
\end{aligned}$$

Where $\frac{\Pr(\alpha \mid \vec{T}_k)}{\Pr(\alpha)}$ is called the *Bayes factor* for a given storm $k$ and parameter $\alpha$. The data-dependent term $C$ is a normalization constant that can be computed so that the pooled posterior is a valid probability distribution integrating to 1. Note that our Bayesian procedure for each storm gives us *samples* from the posterior $\Pr(\alpha \mid \vec{T}_k)$ for each $k$, and $\Pr(\alpha)$ corresponds to the known prior. Thus, to get our pooled posterior estimates $\Pr(\alpha \mid \vec{T}_k)$ for each parameter, we do the following procedure:

1. Fit a normal distribution to the posterior samples for each storm.
2. Calculate the probability density function at each point for the posterior using Equation (5), the above distributions, and the prior distribution.
3. Calculate the posterior summary statistics (95% confidence interval, mean, median) from the calculated probability density function.

Note that, crucially, this procedure does not require refitting models after each storm – we can simply leverage the posterior distributions estimated using each storm's reports separately. After a new storm, we can create an updated pooled estimate without refitting models from other storms.

## A.2 Parameter Estimates for Multiple Storms

We showed in Figure 4 the pooled multivariate regression coefficients from our heterogeneous reporting model. We present results from the individual events—Hurricane Henri, Hurricane Ida, and Tropical Storm Ophelia—that were used to produce these estimates in Figure 5. Estimates for storm-specific parameters ($\theta_0$, $\theta_1$, and $\alpha_0$) were not pooled. The regression coefficient results, however, qualitatively agree across storms: the coefficients do not change direction, but may become statistically significant when pooled. We believe the pooled results are more powerful in providing an interpretation for historical demographic and socioeconomic trends of under-reporting.

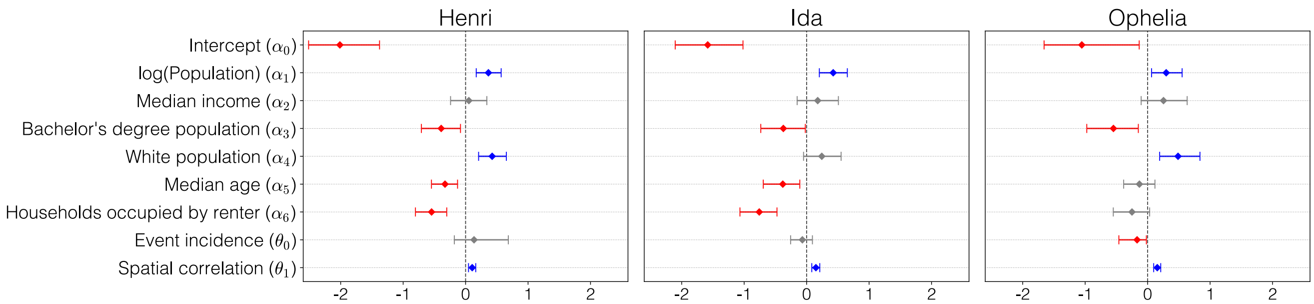


Figure 5: Estimated coefficients for the model trained in each storm individually. For the regression component, all features were standardized to have zero mean and unit variance. Confidence intervals are shown, and estimates with insignificant positive or negative associations are colored in grey.

## A.3 Tract Level Reporting Rates Across Multiple Storms

In the main text, we presented a map of inferred census tract report rates $\psi_i$ in Hurricane Ida (Figure 3). We could infer $\psi_i$ similarly for any of the three storms. Figure 6 shows the resulting scatter plots and correlation. We find a high internal correlation of our method's results across storms. Note that, to compute the pooled report rate, we ignore the intercept $\alpha_0$—whose role is simply to normalize for the average number of observed reports $\vec{T}$—i.e.

$$\psi_i^{\text{pool}} = \text{logit}^{-1}\left(\sum_{\ell=1}^{M} \alpha_\ell^{\text{pool}} X_{i\ell}\right), \tag{6}$$

We also verify that our report rates correlate with previous work on 311 reporting behavior, namely the work of Liu, Bhandaram, and Garg (2023).The correlation with these results is positive but weaker, reflecting the different model estimand and data (reporting rates for tree-related incidents), as well as methodological discrepancies (Liu, Bhandaram, and Garg (2023) use duplicate reports for a given incident).

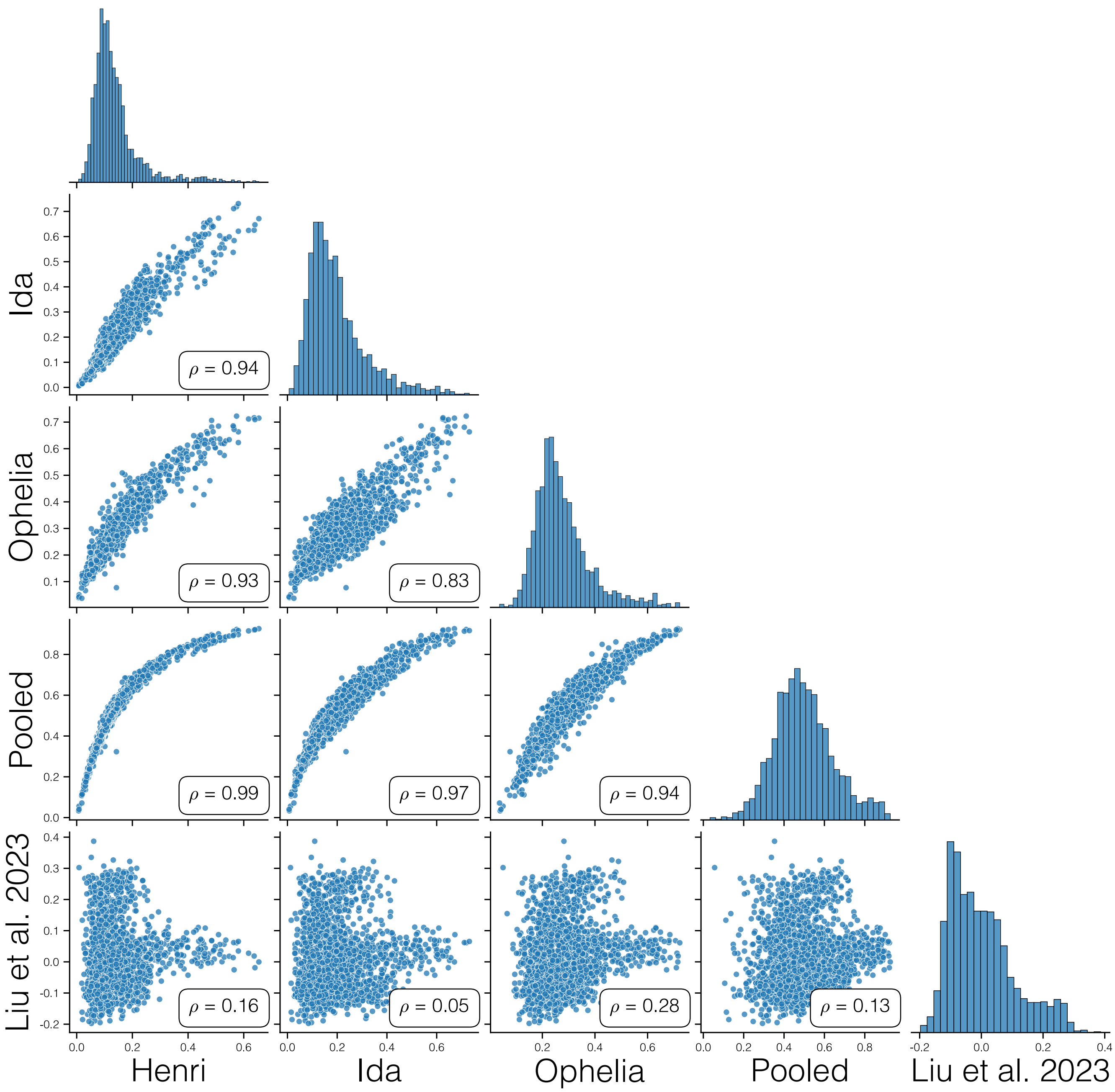


Figure 6: Correlation between the inferred report rates $\psi_i$ per **census tract** for the three different storms considered, as well as the pooled posteriors. The high rank correlation between results for all storms justifies using the pooled results in lieu of results for a specific storm to estimate the report rate. We also include correlations between our model and the model in Liu, Bhandaram, and Garg (2023), previous work focusing on 311 reports of fallen trees.

# B Model Results for Geohash Networks

To verify our results are robust to different graphs (on the same underlying spatial setting), we re-run our models using geohashes. Geohashes encode latitude and longitudes as strings to partition the globe in rectangles of similar areas (see Suwardi et al. (2015) for some properties). We use resolution-6 geohashes and construct a network with $1238$ nodes after pre-processing to remove nodes with high water area and low population. Therefore, our geohash network has around $54\%$ as many nodes as the Census tract network used in our primary results. To associate demographics with each geohash, we project census tract demographic onto the geohash geometry—weighting each tract by the assumed population of the geohash that it contains.

In this section, we show that the model trained on geohashes is consistent (i) within itself, across different storms, and (ii) with the results presented in the main text for the census tract model.

## B.1 Consistency of the Geohash Model Across Multiple Storms

We present results showing that the geohash model is consistent across the three storms considered, mirroring Appendix A. First, Figure 7 shows the parameter estimates inferred from the models. Similar to what we see in Figure 5, most of the regression coefficients $\alpha$ directionally agree across the three storms. We note, however, that the confidence intervals are wider in the case of geohash, resulting in many statistically insignificant coefficients. Increasing the sample size through using resolution-7 geohashes, for example, could address this issue, as there are nearly $50000$ nodes in such graph. However, this procedure would increase model run time and significantly sparsify the reports $\vec{T}$, affecting model priors and other hyperparameters.

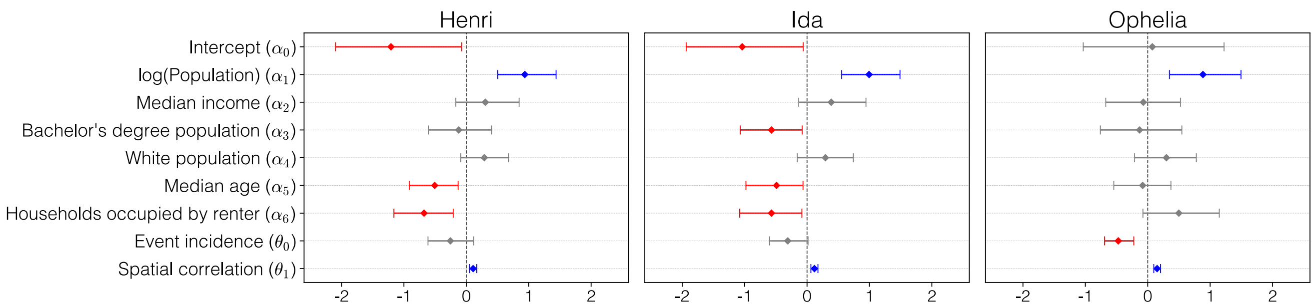


Figure 7: Estimated coefficients for the model trained in each storm individually withe the geohash network. For the regression component, all features were standardized to have zero mean and unit variance. Confidence intervals are shown, and estimates with insignificant positive or negative associations are colored in grey.

Second, we verify in Figure 8 that the predicted report rates for different storms are correlated. We again find positive rank correlation across results for all three storms. We note that we find lower correlation when it comes to Tropical Storm Ophelia (2023). As shown in Figure 7, the regression coefficients for this storm are mostly non significant and four of them have point estimates very close to zero, so that we expect the inferred $\psi_i$ to have high uncertainty.

## B.2 Consistency of the Geohash and the Census Tract Models

We further verify that the geohash models produce estimates consistent with the ones produced by the census tract models, reported on the main text. Figure 9 shows pooled multivariate estimates from geohashes along with main text pooled census estimates. All the coefficients agree directionally, although geohashes produce wider posteriors. Finally, Figure 10 shows that, when we apply the multivariate estimates from each of the model to demographic features, the inferred report rates have positive correlation.

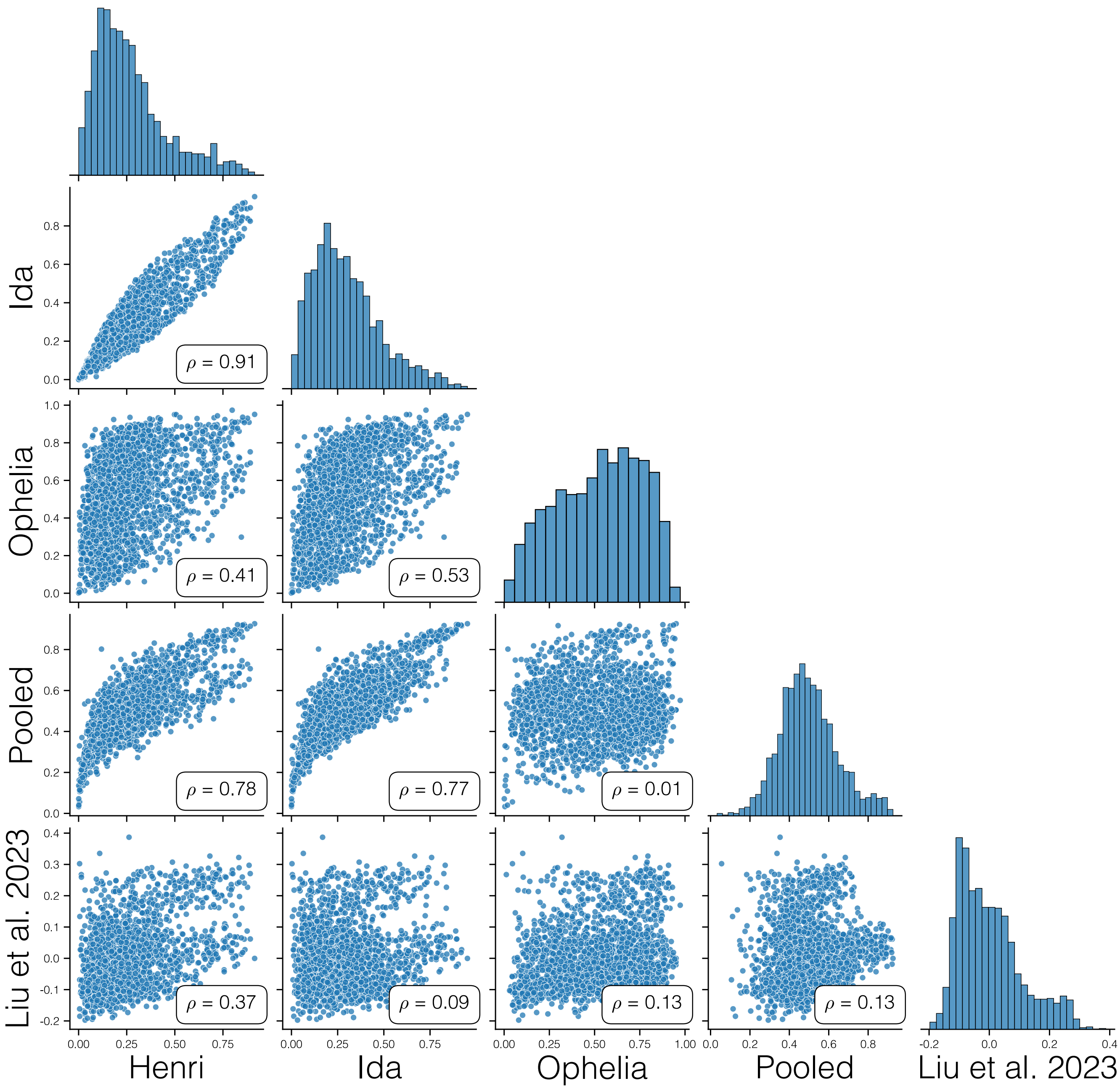


Figure 8: Correlation between the inferred report rates $\psi_i$ per **geohash** for the three different storms considered and the work of Liu, Bhandaram, and Garg (2023). To compute the correlation with the latter, where coefficients are presented per census tract, we apply the estimates attained from geohash models to tract level demographic features.

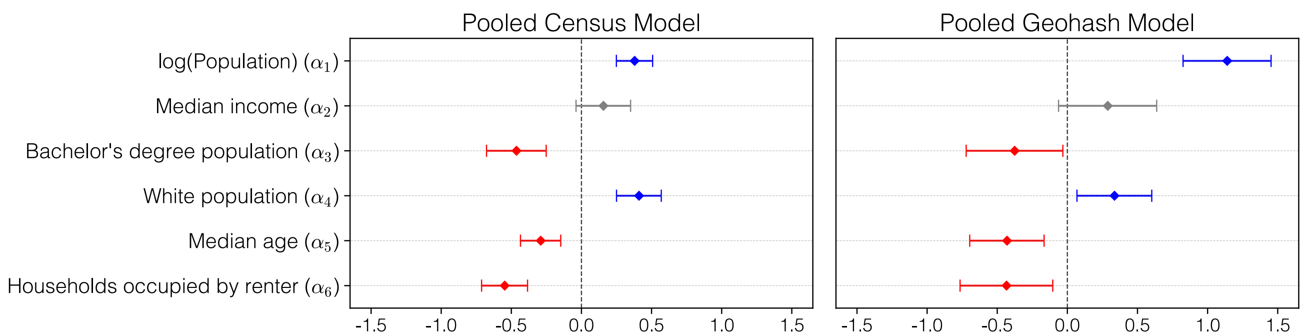


Figure 9: Pooled multivariate coefficients for census tract and geohash models.

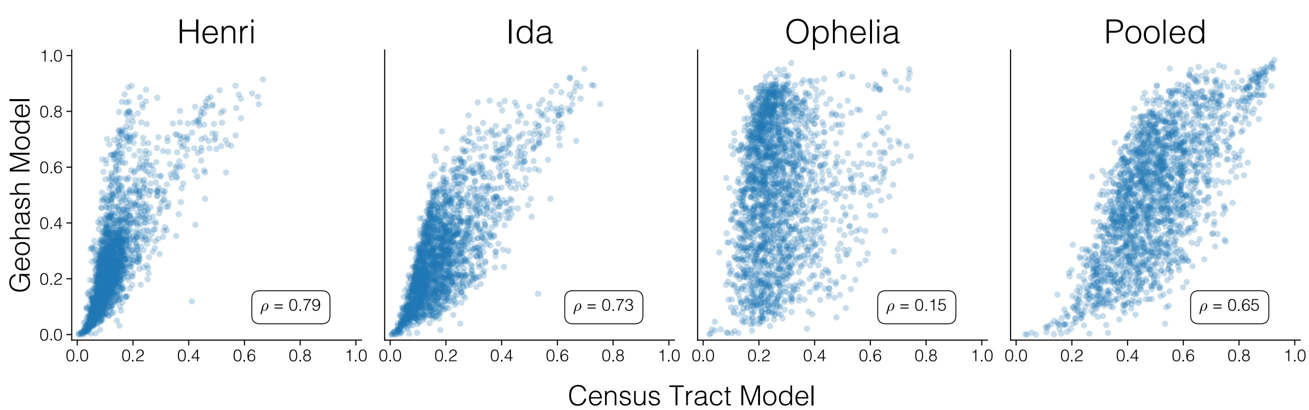


Figure 10: Inferred report rates $\psi_i$ per census tract according to the coefficients estimated by Geohash and Census Tract Models in each of the storms as well as for the pooled model.

## C Univariate Heterogeneous Reporting Models

In our primary analyses, we report the result of *multivariate* reporting coefficients, i.e., include both population and income in the same model. A standard limitation of such an approach is that these coefficients have high co-linearity in NYC, limiting interpretation. We further cannot use the findings from Figure 4 to report associations between each feature and the report probability. Additionally, many other features of interest were not included, so as to not to incur further co-linearity.

To address these issues, we train our heterogeneous reporting models with *one socioeconomic or demographic feature at a time*. These univariate models present faster convergence than the full heterogeneous reporting model presented on the main text. We draw 15,000 samples from three chains, after 10,000 burn-in samples. All other sampling hyper-parameters remain the same—including the network.

Figure 11 shows the pooled results for the census tract and the geohash networks. Patterns from Figure 3 re-emerge on census tracts: reports are heavily skewed along racial lines for census tracts, where a higher percentage of White or Asian residents correlates positively with report probability but a higher percentage of Hispanic or Black residents correlates negatively. Similarly, neighborhoods with higher populations, higher median incomes, and higher proportion of owner-occupied households tend to report events at higher rates than other areas.

One difference between the models is the coefficients for population density (either population normalized by total node area or just by the land area). The census tract model learns negative coefficients for these values, which may be against intuition (more people who can report the same flooded area should increase reporting probability). This negative coefficient shows a limitation of our current Bayesian model: it assumes that the prior probability that each node is flooded $P(A)$ is the same – even if, e.g., some nodes are larger (so more potential area to be flooded) or in lower lying areas. Thus, if a larger land area (lower population density) is more likely to flood *conditional on the flooding reports of neighbors*, the model fits this via higher reporting rates. As geohashes have extremely similar land areas, this effect does not appear in the geohash model (and so population density and population data are very similar). Model changes that incorporate such differential priors as a function of node characteristics are a step for future work; we note that all our primary results, as reported in the main text, are consistent between the geohash and census data preprocessing.

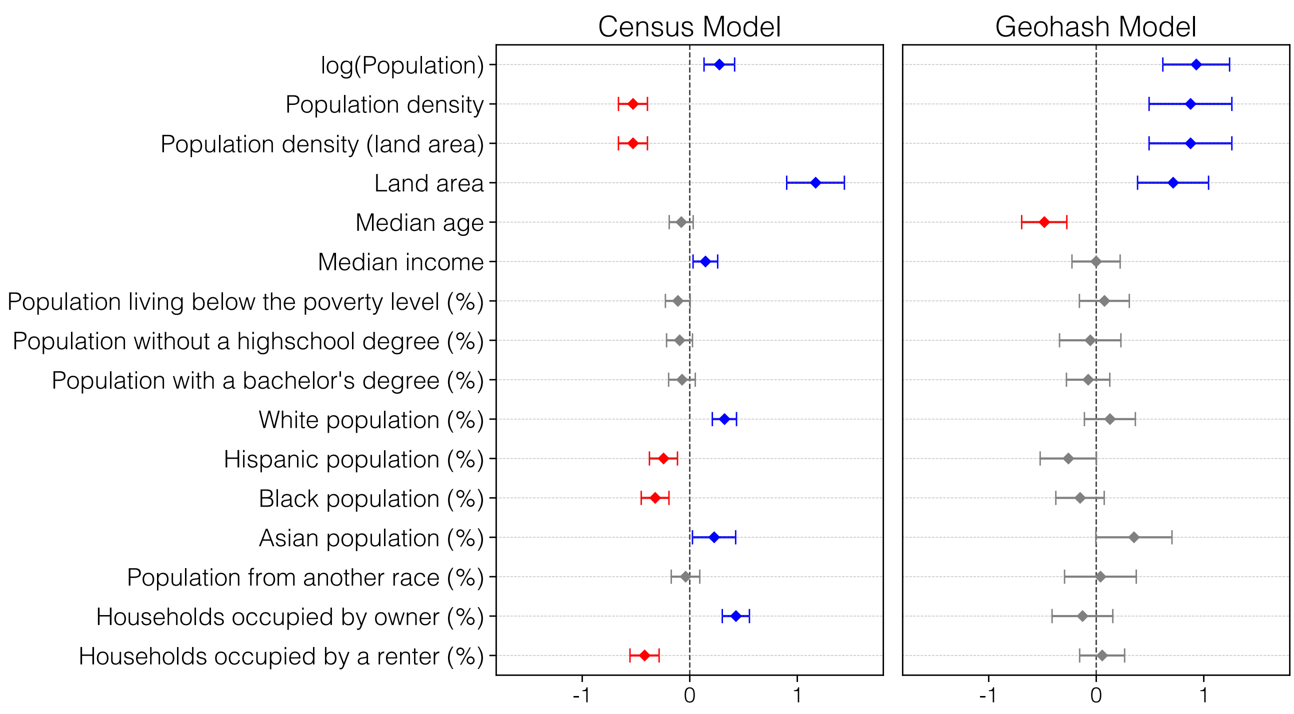


Figure 11: Estimated effect of each demographic feature on reporting rate, according to the pooled posterior for each of the networks. Covariates were standardized prior to fitting the model.

Overall, other results directionally agree between the census tract and geohash models. However, most of the geohash correlations are not statistically significant. We attribute this to (1) the lower network size in the case of geohashes, and so fewer data for the associated parameter estimation, and (2) the fact that geohash geometries are not delineated to consider some demographic coherence such as ensuring similar population counts or respecting physical and geographic boundaries—resulting in noisy measurements. These univariate results are consistent across storm—although noisier on the geohash setting, as expected—as shown by Figure 12.

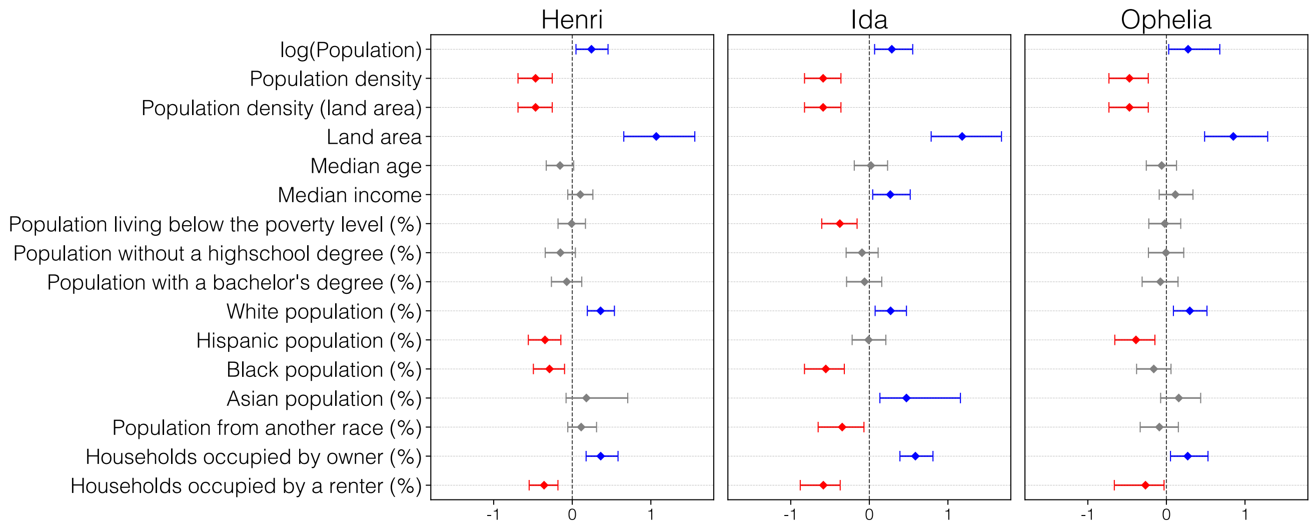


(a) Results for the **census tract** network models

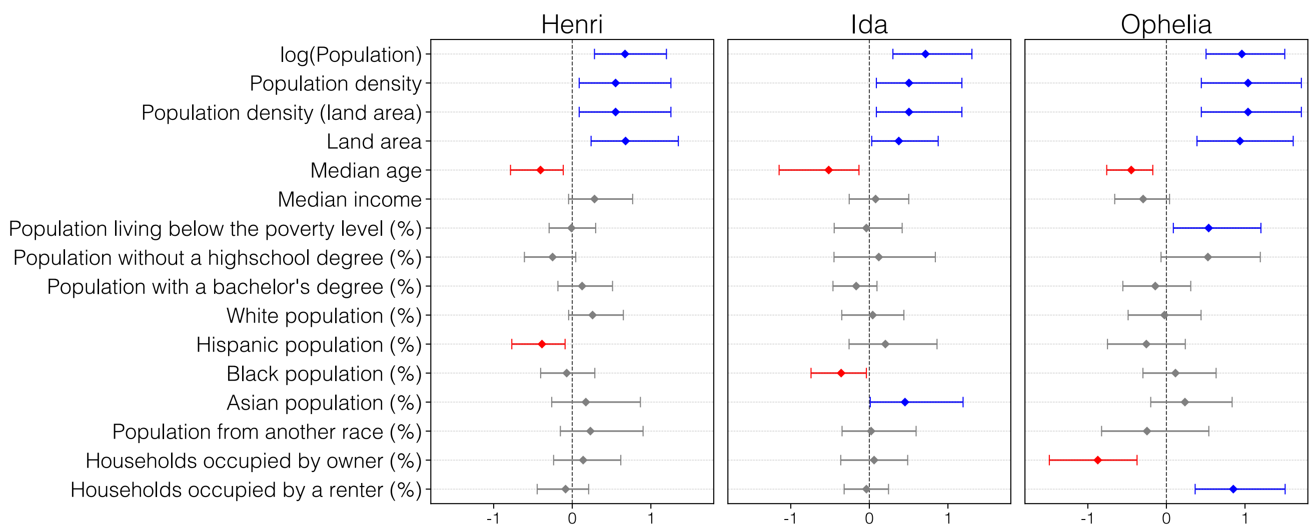


(b) Results for the **geohash** network models

Figure 12: Estimated effect of each demographic feature on reporting rate for each storm according to the (a) census tracts and (b) geohash models.

## D Further Details on Semi-Synthetic Simulation Experiments

We now report additional results with our semi-synthetic simulations. Recall that these experiments use the real census tract network and associated demographic features. However, instead of using real report data $\vec{T}$, we simulate ground-truth $\vec{A}$ and report data $\vec{T}$, *assuming* that either the homogeneous reporting or heterogeneous reporting models are correctly specified. In the former case (drawing data according to the homogeneous reporting model), we sample $\theta_0, \theta_1, \alpha$ from their prior distributions, and then use those values to draw $A_i$, $T_i$ for all nodes $i$. In the latter case (drawing data according to heterogeneous reporting model), we sample $\theta_0, \theta_1, \{\alpha_\ell\}$, and then draw $A_i$, $T_i$.

### D.1 Calibration and Identifiability

First, we illustrate the calibration and identifiability findings. Figure 13 shows that both models approach perfect calibration on all latent parameters. We then report parameter identifiability results when the simulated data is drawn from the homogeneous model, and from the heterogeneous model. As the Pearson correlation coefficients $\rho$ illustrate in Figure 14, the inferred posterior means are well-correlated with the true parameters. Accurate estimation of the $\alpha_\ell$ is especially important, as these parameters correspond to relative reporting behavior as a function of demographics.

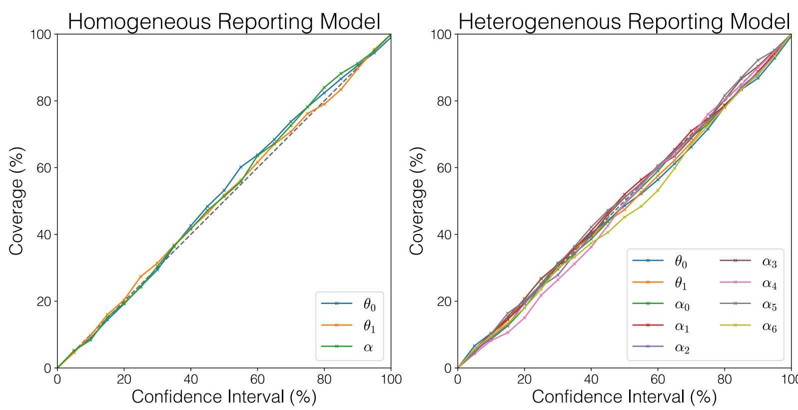


Figure 13: Calibration of synthetic experiments with each of the homogeneous and the heterogeneous reporting models. Point $(x, y)$ corresponds to the $x\%$ confidence interval of the parameter's posterior distribution containing $y\%$ of the ground truth parameters. A perfectly calibrated model lies along the diagonal line.

### D.2 Predictive Performance

We report the AUC and RMSE for our semi-synthetic simulations. We measure the ability of our model to recover *the latent ground-truth* $A_i$ of each node. In all evaluations, nodes that did report during the training period (i.e. $T_i = 1$) are excluded as these nodes are perfectly predicted by all models by definition.

Table 3 shows results for data generated from the homogeneous reporting model i.e. assuming a constant report rate throughout the graph. All three models over-perform random classification, with evidence that our model—the only one which directly accounts for under-reporting—performs better than the two baseline models.

| **Model** | **AUC Estimate** | **AUC 95% CI** | **RMSE Estimate** | **RMSE 95% CI** |
|---|---|---|---|---|
| Homogeneous Reporting | 0.577 | (0.573, 0.580) | 0.400 | (0.390, 0.410) |
| GP Baseline | 0.536 | (0.533, 0.539) | 0.494 | (0.482, 0.506) |
| Spatial Baseline | 0.558 | (0.554, 0.561) | 0.463 | (0.450, 0.477) |

(a) AUC and RMSE point estimates and confidence intervals for each of the three models.

| **Model A** | **Model B** | $\Delta_{\text{AUC}}$ | **AUC p-value** | $\Delta_{\text{RMSE}}$ | **RMSE p-value** |
|---|---|---|---|---|---|
| Homogeneous Reporting | GP Baseline | 0.041 | $< 10^{-4}$ | -0.094 | $< 10^{-4}$ |
| | Spatial Baseline | 0.019 | $< 10^{-4}$ | -0.063 | $< 10^{-4}$ |

(b) AUC and RMSE changes. The p-values correspond to a two-sided test that Model A and Model B perform differently.

Table 3: Performance metrics when the data is generated with **homogeneous under-reporting**. Confidence intervals were obtained through bootstrapping the tracts with 10,000 iterates.

When we simulated data according to the heterogeneous reporting model, we additionally compared the performance of the (correctly specified) heterogeneous reporting model to the homogeneous reporting model and the baselines. Table 4 shows that accounting for difference in report rates leads to significant improvements on predicting latent ground truth.

| **Model** | **AUC Estimate** | **AUC 95% CI** | **RMSE Estimate** | **RMSE 95% CI** |
|---|---|---|---|---|
| Heterogeneous Reporting | 0.642 | (0.637, 0.647) | 0.378 | (0.369, 0.386) |
| Homogeneous Reporting | 0.520 | (0.515, 0.525) | 0.464 | (0.450, 0.478) |
| GP Baseline | 0.501 | (0.497, 0.505) | 0.512 | (0.499, 0.524) |
| Spatial Baseline | 0.513 | (0.509, 0.518) | 0.487 | (0.472, 0.501)) |

(a) AUC and RMSE point estimates and confidence intervals for each of the three models.

| **Model A** | **Model B** | $\Delta_{\text{AUC}}$ | **AUC p-value** | $\Delta_{\text{RMSE}}$ | **RMSE p-value** |
|---|---|---|---|---|---|
| Heterogeneous Reporting | Homogeneous Reporting | 0.123 | $< 10^{-4}$ | -0.087 | $< 10^{-4}$ |
| | GP Baseline | 0.142 | $< 10^{-4}$ | -0.134 | $< 10^{-4}$ |
| | Spatial Baseline | 0.129 | $< 10^{-4}$ | -0.109 | $< 10^{-4}$ |
| Homogeneous Reporting | GP Baseline | 0.019 | $< 10^{-4}$ | -0.030 | $< 10^{-4}$ |
| | Spatial Baseline | 0.007 | 0.042 | -0.022 | 0.025 |

(b) AUC and RMSE changes. The p-values correspond to a two-sided test that Model A and Model B perform differently.

Table 4: Performance metrics when the data is generated with **heterogeneous under-reporting**. Confidence intervals were obtained through bootstrapping the tracts with 10,000 iterates. The AUC estimates are repeated from main text.

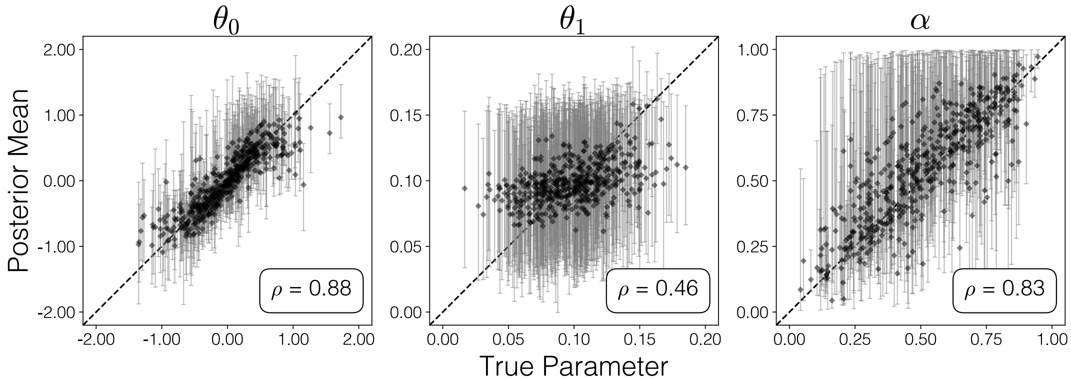


(a) Results for the **homogeneous reporting** model

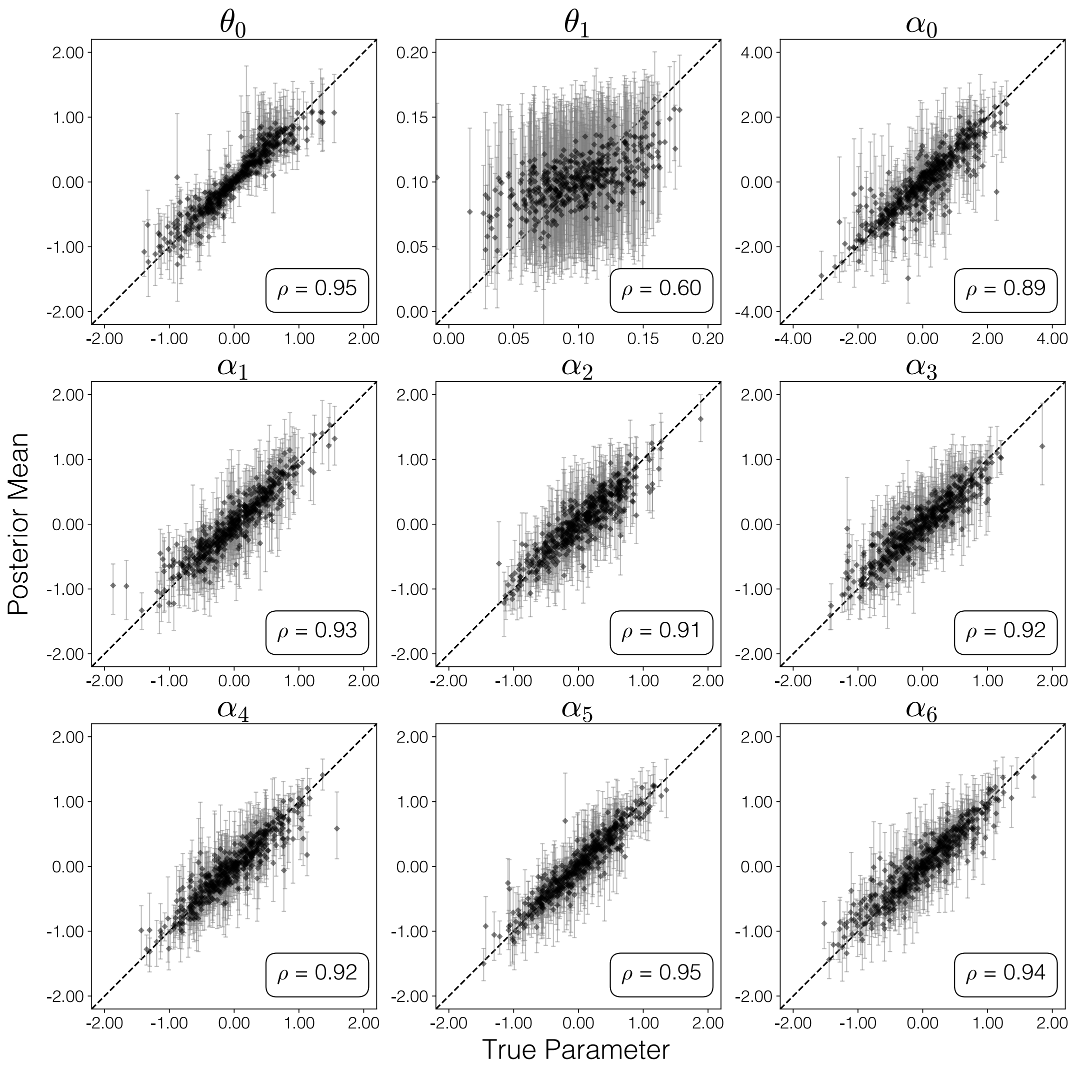


(b) Results for the **heterogeneous reporting** model

Figure 14: Recovery of parameters in simulation in the well-specified (a) homogeneous and (b) heterogeneous reporting models. Vertical axes corresponds to inferred parameter posterior, and horizontal axes to the true parameter value—so that a perfect model would lie along the diagonal. Error bars correspond to $95\%$ confidence intervals of the posteriors.

## E Further Details on the Equity Allocation Analysis

Qualitatively, the improvements in equity are independent of the number of inspected Census tracts and the socioeconomic or demographic factors considered. We showed in Figure 2 that the heterogeneous reporting model allocates inspection resources to un-reported census tracts more in line with the population distribution than the homogeneous reporting model along the lines of race and education, when the agency hypothetically would inspect 100 tracts in order of highest posterior probability of a flood. In Figure 15, we extend this result to more socioeconomic factors as well as different numbers of inspected census tracts.

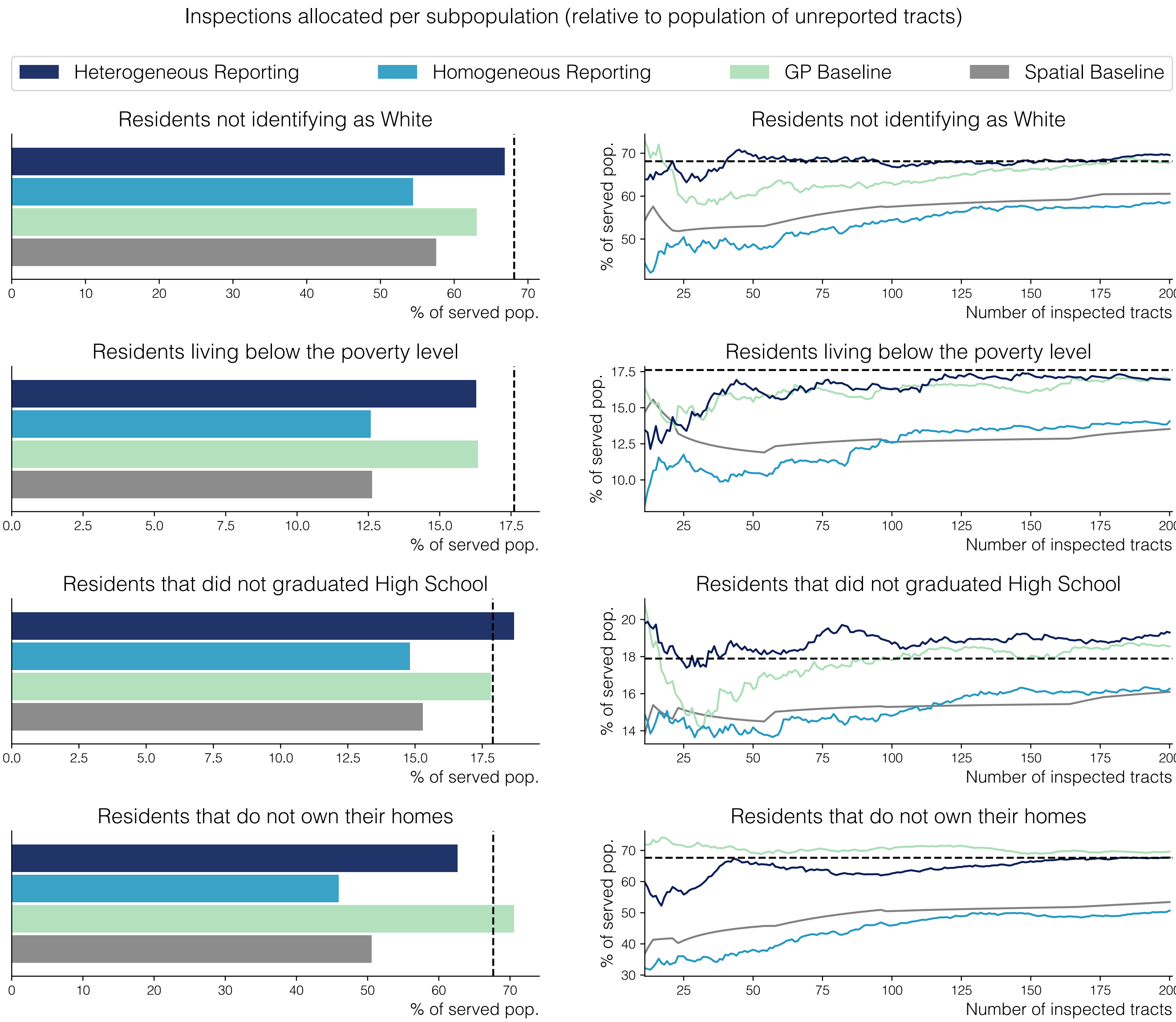


Figure 15: Percentage of non-white, below poverty level, without a high school degree, and household renter populations that are served by inspections of 100 unreported census tracts—along with a line plot of these values for varying numbers of inspected tracts. Dashed lines correspond to the underlying sub-population percentage living on tracts that did not receive a report.

Regardless of the number of inspected tracts (after an initial, noisy period), the sub-population rates inspected according to the heterogeneous model and the GP baseline better approach the underlying population base rate than the other models. The GP baseline does so while achieving poor overall performance—as discussed in Table 2 (i.e., inspecting tracts close to at random)—whereas the heterogeneous reporting model simultaneously achieves high performance and equity.

Note also that the lines for the spatial baseline model are smoother due to tie-breaking: many tracts have the exact same fraction of their neighbors with a report, and when that happens there is a chance we cannot fit tracts with the same priority in the inspection capacity. We weigh the tracts at the last position equally to fill all the leftover spots.

# F Further Details on Model Parameters

## F.1 Model Priors

**Event prevalence $\theta_0$** We assume a centered normal prior of the form:

$$\theta_0 \sim \mathcal{N}\,(0, 0.5)$$

**Spatial correlation $\theta_1$** We assume a non-negative normal prior of the form:

$$\theta_1 \sim \mathcal{N}\,(0.1, 0.03)$$

We make two important comments about this prior. First, it forces the spatial correlation to be likely positive; Zero spatial correlation leads to a non-identifiable PU model, and as shown in the data generation experiments, negative spatial correlation—which is not common in the application we leverage—produces a significantly tighter range of latent states $\vec{A}$ regardless of the $\theta_0$ value. Second, although this prior distribution has low standard deviation, the joint distribution of $\theta_0$ and $\theta_1$ generates vectors $\vec{A}$ whose average spans most of the $(-1, 1)$ interval as shown in Figure 16—suitable therefore for real-world data settings.

**Regression coefficients $\alpha_\ell$** We assume centered normal prior distributions of the form:

$$\alpha_0 \sim \mathcal{N}(0, 1.0) \quad \alpha_\ell \sim \mathcal{N}(0, 0.5)$$

**Homogeneous Report Rate $\alpha$** With homogeneous reporting, we impose a loose Beta prior on $\alpha$:

$$\alpha \sim \text{Beta}(1.2, 0.8)$$

We confirm that our prior choices are not *restrictive* – that they can represent a full range of data. Through Figure 16 we show that our spatial correlation $\theta_1$ and location $\theta_0$ parameters can together generate a full range of the fraction of nodes that are positive with the assumed priors.

## F.2 Sampling Hyperparameters

Each of our chains follows:

- The **number of MCMC iterations** used is 60,000.
- The **number of burn-in iterations** used is 20,000.
- The **thinning fraction of post burn-in MCMC iterations** used is 0.5.

The SVEA is implemented following Møller et al. (2006).

- The **number of SVEA iterations** per MCMC iteration is 1.
- The **number of burn-in samples in the Swendsen-Wang algorithm** used to generate the auxiliary variable is 50.
- The **initial proposal step size** $\sigma$ on the distribution $\theta_{\text{NEW}} \sim \mathcal{N}(\theta_{\text{OLD}}, \sigma)$ is 0.2.
- The stepsize is adapted **every** 50 **MCMC iterations** if the acceptance rate is not between 0.25 and 0.60. The multiplicative factor is 0.15—either decreasing or increasing the current stepsize, depending on whether we were under-accepting proposals or over-accepting respectively.
- The **parameter initialization** takes the current parameter values for both the $\theta$ parameters and the auxiliary variables (taking current $\vec{A}$ values).

The Bayesian logistic regression sampling is implemented with PyMC.

- The **number of burn-in iterations** per MCMC iteration is 50.
- The **parameter initialization** takes the current parameter values.

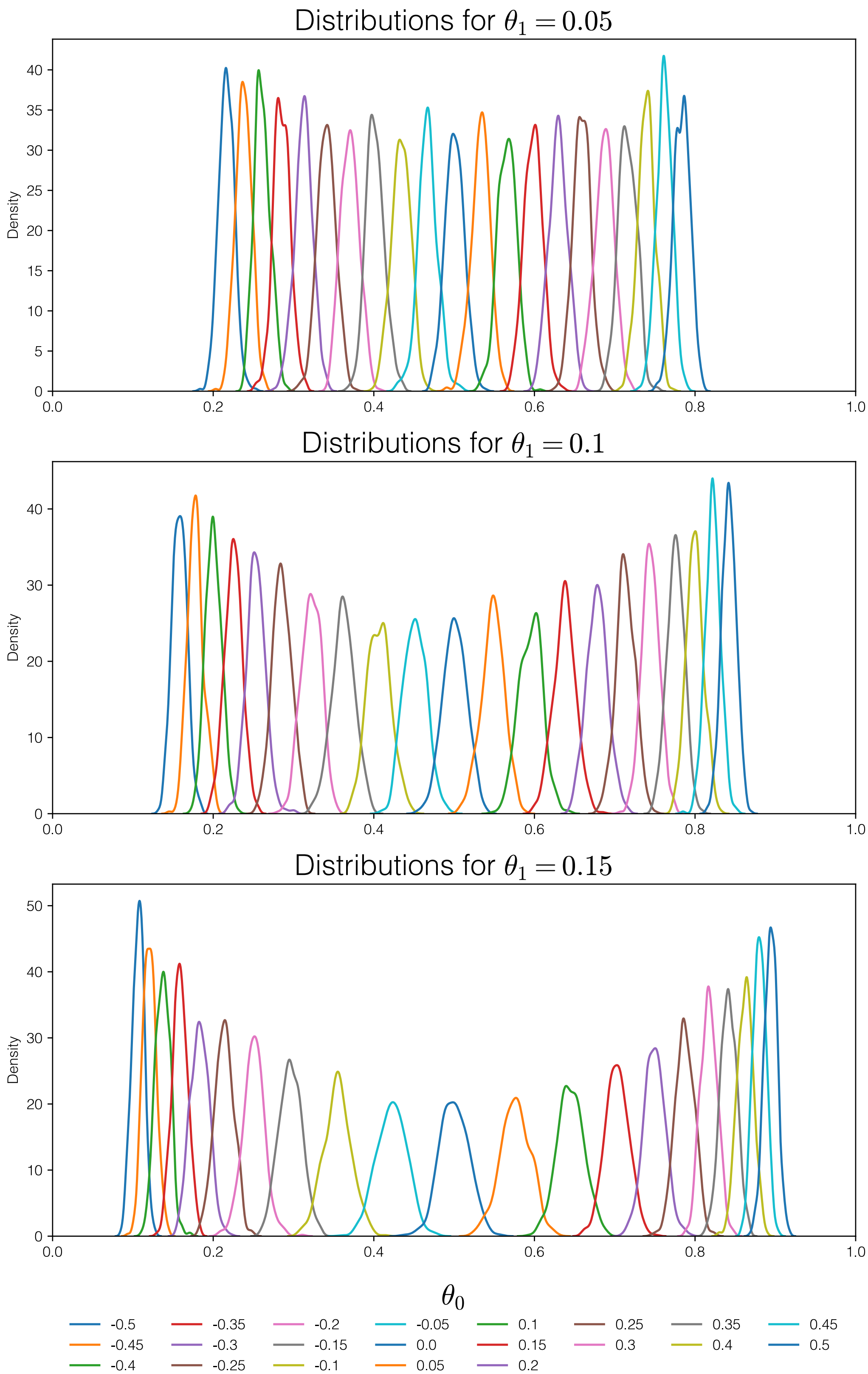


Figure 16: Estimated densities for the fractions of nodes with $A_i = 1$ for different choices of $\theta_0$ and $\theta_1$. We generated $500$ samples per pair of parameters.

## G Further Details on Data

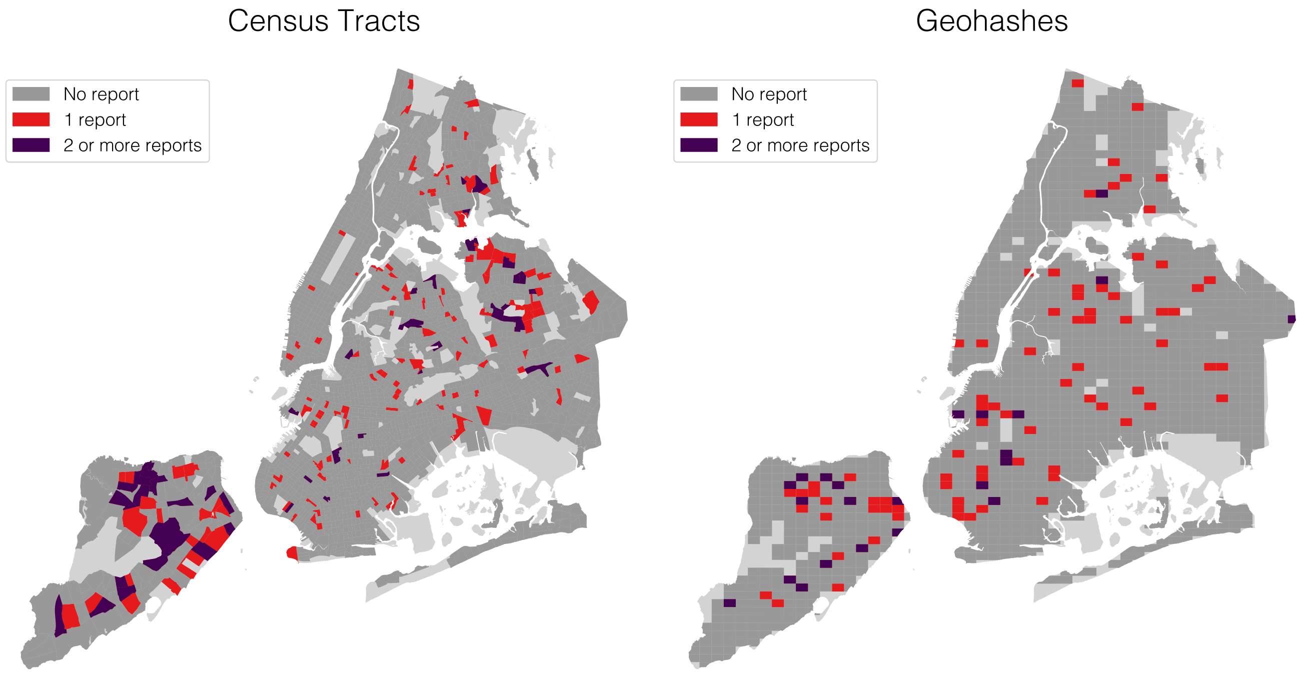


Figure 17: Counts of reports during the training period for Hurricane Ida for both networks. Locations in grey received no report. We note that most of the reported tracts have only one or very few reports, validating our use of only the presence of any reports. Because there is a different number of geohashes and census tracts yet we keep a fixed rate of 8% of units reporting in the training period, some census tracts with reports have no corresponding reported geohashes.

| Feature | Average | sd |
|---|---|---|
| log(Population) | 8.162 | 0.519 |
| Population density (per $m^2$) | 0.021 | 0.014 |
| Land area ($m^2$) | 283,996 | 396,845 |
| Median age | 37.9 | 5.8 |
| Median income | \$ 73,909 | \$ 37,072 |
| Population living below the poverty level (%) | 16.4 | 12.2 |
| Population without a high school degree (%) | 17.4 | 11.4 |
| Population with a bachelor's degree (%) | 36.9 | 21.3 |
| White population (%) | 30.3 | 27.3 |
| Hispanic population (%) | 26.9 | 21.0 |
| Black population (%) | 21.7 | 25.8 |
| Asian population (%) | 15.7 | 17.4 |
| Population from another race (%) | 1.7 | 2.7 |
| Households occupied by the owner (%) | 37.26 | 26.0 |
| Households occupied by a renter (%) | 61.0 | 26.0 |

Table 5: All demographic and socioeconomic features used in the heterogeneous reporting model. Data was obtained from the 2020 Decennial Census. Land area was computed from the geometry. Percentage columns are normalized by the total population (or households) of the Census tract—and tracts with no population are excluded. All features were standardized prior to model fitting. For the full model, we used six features: log(Population), median age, median income, population with a bachelor's degree, white population, and households occupied by the owner.

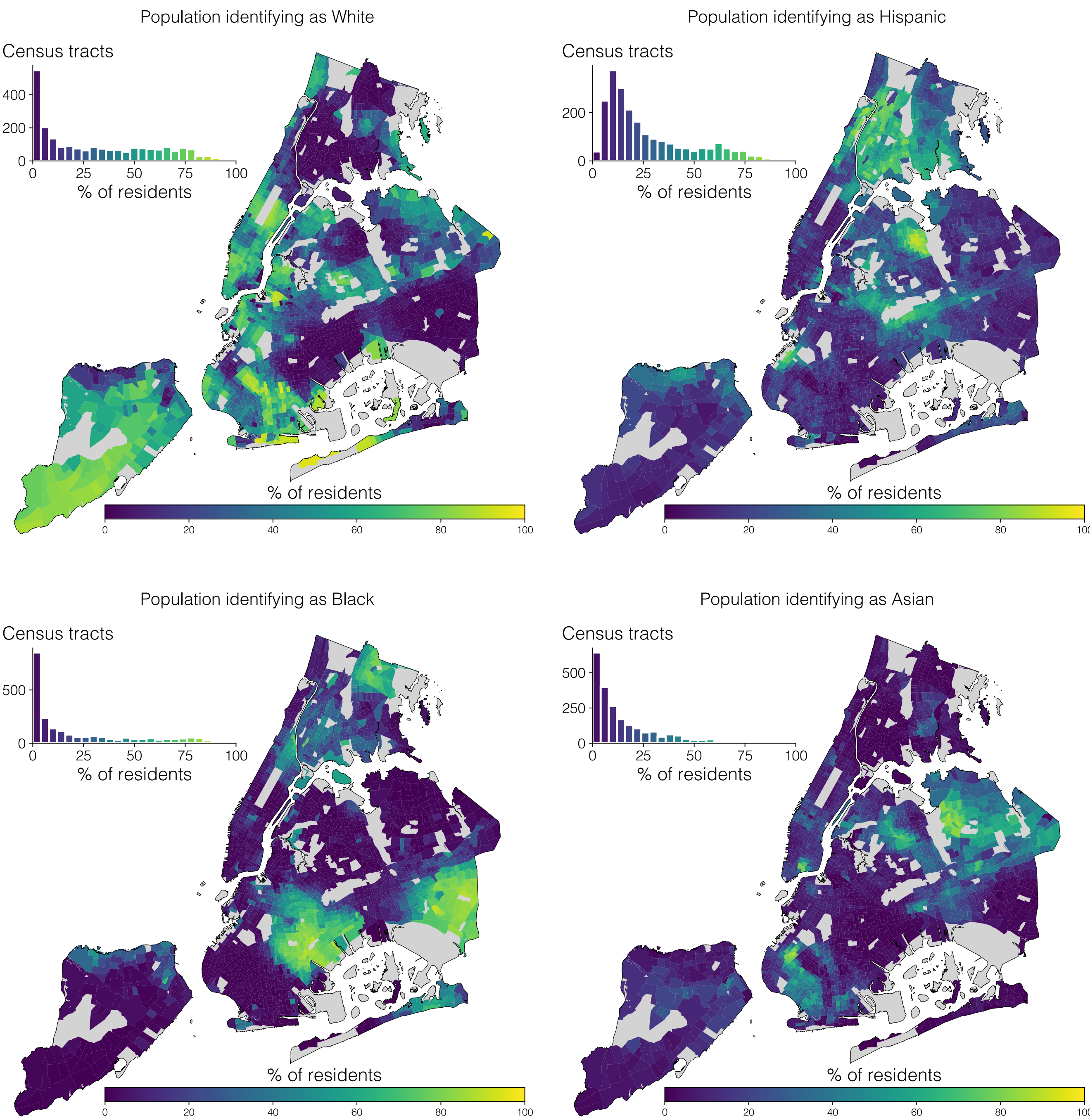


Figure 18: Race and Ethnicity in New York City per Census tracts. Each map shows the proportion of tract residents identifying as (a) White (b) Hispanic (c) Black and (d) Asian. As shown, this is a very spatially correlated feature, possibly due to systemic patterns of segregation. As seen in the histograms counting the number of tracts according to their percentage of subpopulation residents, the Hispanic population is more dispersed compared to Black and Asian populations, i.e. few tracts have zero Hispanic residents.